

## Award Accounts

The Chemical Society of Japan Award for 2005

# Time-Resolved Spectroscopic and Imaging Studies on Laser Ablation of Molecular Systems: From Mechanistic Study to Bio/Nano Applications<sup>#</sup>

Hiroshi Masuhara

Department of Applied Chemistry and Institute of Molecular Science, National Chiao Tung University,  
Ta Hsueh Rd. 1001, Hsinchu 30010, Taiwan

Received March 5, 2013; E-mail: masuhara@masuhara.jp

Studies on laser ablation of polymer films, molecular crystals in solution, protein solution, and culture media containing living cells are summarized and considered. Dynamics and mechanism of laser ablation were systematically studied by utilizing time-resolved spectroscopy and imaging; femtosecond–nanosecond transient absorption and emission spectroscopy, nanosecond shadowgraphy, nanosecond–nanometer interferometry, femtosecond surface light scattering imaging. It was confirmed by integrating both data that primary processes of laser ablation can be well understood in the framework of Jablonski diagram. For nanosecond laser ablation of doped polymers, it was demonstrated that cyclic multiphoton absorption is an efficient photothermal conversion process leading to photothermal ablation. For femtosecond laser ablation of dye films, transient pressure mechanism was proposed indicating photomechanical ablation. As applications of laser ablation, nanoparticle preparation, protein crystallization, and manipulation of living cells are presented. Laser ablation of molecular crystals in poor solvent gives small fragments whose size are in a few tens nm. The fabricated nanocolloids are stable without adding detergents and their size was the smallest as nanoparticles produced by the top-down-method. Multiphoton laser ablation of water generates local impulsive force due to bubble formation, shockwave propagation, and local convection flow. The force triggers molecular and protein crystallization in their supersaturated solutions, whose mechanisms are described and considered. The impulsive force is also very useful for manipulating living cells and its high potential was confirmed by examining cell functions such as division, differentiation, death, and migration. Finally summary and future plan are presented.

Studies on molecular spectroscopy and photochemistry introduced lasers very early in 1960's and used them as light sources for spectroscopic measurements as well as for inducing photochemical reactions. When chemists started to use pulsed lasers, they soon became aware that laser irradiation induced vaporization, decomposition, and fragmentation of materials and found that the irradiated surface was etched. The left patterns on the colored papers were practically used to confirm optical alignment in experimental setups before infrared (IR) viewer became popular. Later this laser-induced phenomenon was called laser ablation by Srinivasan,<sup>1</sup> and its systematic application was quickly developed to fabricate microstructures of various materials by electronics engineers and to microsurgery by medical doctors. Laser ablation is made possible by applying pulsed lasers and never brought out by weak continuous wave (CW) laser even when its irradiation continues for 1 year. Laser ablation is one of representative nonlinear photochemical phenomena and has a threshold with respect with laser fluence. Initially most of laser ablation studies were carried out for metals, semiconductors, ceramics, and glasses,<sup>2</sup> while organic materials,<sup>3–6</sup> cells, tissues, and organs have recently been receiving more and more attentions.<sup>7</sup>

In general ablation mechanism of organic and bio materials was discussed from photochemical and photothermal viewpoints. The former was simply expected, as multiphoton excitation energy is sometimes higher than ionization potential and chemical bond energy, leading to ion formation and bond cleavage, respectively. The molecules in the irradiated volume may decompose typically to small gas phase molecules and the volume should be etched. This interpretation is due to thermodynamic consideration and time scale at which the decomposition takes place is not examined. When the relaxation from the higher excited states to the first excited state is fast, the excess energy is converted to heat before ionization and decomposition takes place from the higher excited states. The irradiated area is instantaneously heated to high temperature and shows explosive melting, leading to fragmentation and ejection. This decomposition behavior is interpreted as photothermal ablation. At the early stage of ablation studies of molecular materials, such mechanistic considerations seemed reasonable and were presented in many papers.<sup>1–8</sup> From theoretical viewpoints some photothermal models were presented for polymer ablation, taking into account the movement of the interface between initial solid and product gaseous phases.<sup>9,10</sup> On the

other hand a simple sublimation model was proposed assuming the similarity between polymers and inorganic materials,<sup>11,12</sup> which was later developed to discriminate various models.<sup>13</sup> Further systematic studies on cryogenic molecular solids and liquids were extended, leading to deep understanding on laser ablation mechanism of molecular materials.<sup>14</sup>

It is not easy to conclude on ablation mechanism in general, as ablation behavior is dependent on laser fluence, wavelength, pulse width, repetition rate, and total shots of laser pulses, and of course on materials properties as well as their surface and environmental conditions. Most of ablation studies had been done for practical applications, so that exact mechanistic approach was relatively limited. We considered that the time-resolved spectroscopic measurements are necessary and indispensable to reveal how electronic excitation energy is used for material ejection, what chemical species are involved, and in what time scale electronic excitation evolves to morphological changes. Such spectroscopic measurements have been combined with newly developed time-resolved imaging, whose results have given us better pictures of laser ablation dynamics and mechanism at the molecular level. Furthermore the results on time-resolved studies have led to various proposals of laser-based tools, methods, and technologies. Now laser ablation studies are growing up to new research horizons where molecular implantation, molecular and protein crystallization, growth control of crystals, patterning of protein cubes, or even manipulation of living cells in solution become contemporary topics.

In the present Account our systematic studies on laser ablation utilizing time-resolved spectroscopy and imaging are summarized and discussed in view of photophysics and photochemistry. In Section 1, nanosecond laser ablation dynamics and mechanism are described, where experimental results were obtained by nanosecond emission and absorption spectroscopies, time-resolved shadowgraphy, and nanosecond-nanometer interferometry. Photothermal expansion/contraction dynamics and photochemical ablation are summarized for polymer films. In Section 2, the results on femtosecond laser ablation dynamics and mechanism are presented, which are all based on ablation phenomena induced by irradiation with a 100 fs Ti:sapphire laser pulse. In Section 3, nanoparticle preparation in solution is introduced as practical outputs from our laser ablation study and demonstrated to have high potential in nanomaterials research. In Section 4, as another interesting output, crystallization and crystal growth by femtosecond laser ablation is described and considered. In Sections 5 and 6, we summarize on femtosecond ablation of solution giving local impulsive force with bubble formation and describe on its application to crystal growth and crystallization of molecules and proteins by the bubbling. In Section 7, it is summarized how living cells in solution can be manipulated by the laser-induced bubbling, where the cells are not irradiated directly. It is worth to note that whole manipulation can be done in solution without exposing cells to air. Summarizing these results and our ideas, we will present our perspective on laser ablation studies in molecular systems.

## 1. Nanosecond Laser Ablation Dynamics and Mechanism

For elucidating dynamics and mechanism of molecular excited states under laser ablation condition, it should be useful

to correlate primary processes of laser ablation with well known photophysical and photochemical properties of molecules. From this viewpoint we chose aromatic molecules such as biphenyl, *p*-terphenyl, *N,N,N',N'*-tetramethyl-*p*-phenylenediamine, carbazole, anthracene, and pyrene, and doped them in polymer films.<sup>15–41</sup> Furthermore photoreactive groups were chemically bonded into polymers chains, and their films were formed.<sup>42–49</sup> Ablation is initiated by absorption of excitation photons by those dopants, and their dynamics was studied by applying time-resolved absorption and fluorescence spectroscopy, transmittance measurement at excitation wavelength, time-of-flight mass spectroscopy, nanosecond shadowing, and photoacoustic measurement. In general no appreciable decomposition product indicating photochemical ablation mechanism was detected and photothermal conversion was considered to be responsible to the fragmentations. The excited states of dopant molecules were detected spectroscopically, molecular radicals suggesting photodecomposition were not identified, temperature elevation was confirmed by analyzing fluorescence spectral broadening and time-of-flight mass spectrometry, and surface morphology suggesting melting of ablated area was observed after ablation. Furthermore time-resolved interferometry clarified expansion and contraction dynamics before fragmentation and ejection take place. These experimental results indicate that the excited molecules convert electronic excitation energy to intermolecular and lattice vibrations very efficiently without appreciable chemical decomposition of dopants. On the basis of these results, we proposed photochemical mechanism based on “cyclic multiphotonic absorption” for aromatic molecule-doped polymers.

On the other hand, when photodecomposable groups are introduced to main chains or side substituents of polymers, ablation behavior is much changed. Upon densely electronic excitation of the polymers with high intensity laser pulse, very rapid dissociation is induced densely and polymer morphology cannot be maintained anymore, undergoing the etching in the irradiated area, which can be assigned as photochemical ablation. The specially designed polymers are necessary for confirming photochemical ablation and we used nitrocellulose, triazene polymer, polyurethane, and polyimide films. Also we found that their ablation sometimes involves combustion and detonation, which is one of extreme cases of the photochemical ablation. Here our experimental results demonstrating nanosecond photochemical and photochemical ablation are summarized and considered.

**1.1 Spectroscopic Study of Laser Ablation of Doped Polymer Films.** In laser ablation sample films are etched efficiently, so that the decomposed materials, molecules, atoms, and so on should be ejected to air. Under such condition it was believed that transient absorption spectral measurement was much disturbed. Also plasma emission is frequently observed, which was considered to make transient absorption spectral measurement difficult. However, by conducting various time-resolved measurements including time-resolved shadowgraphy, we found these experimental difficulty is not critical in observing transient species at early stages of laser ablation, namely, ejection occurs relatively later and the primary processes of laser ablation can be probed not being so much disturbed optically by the dispersed materials. As an exam-

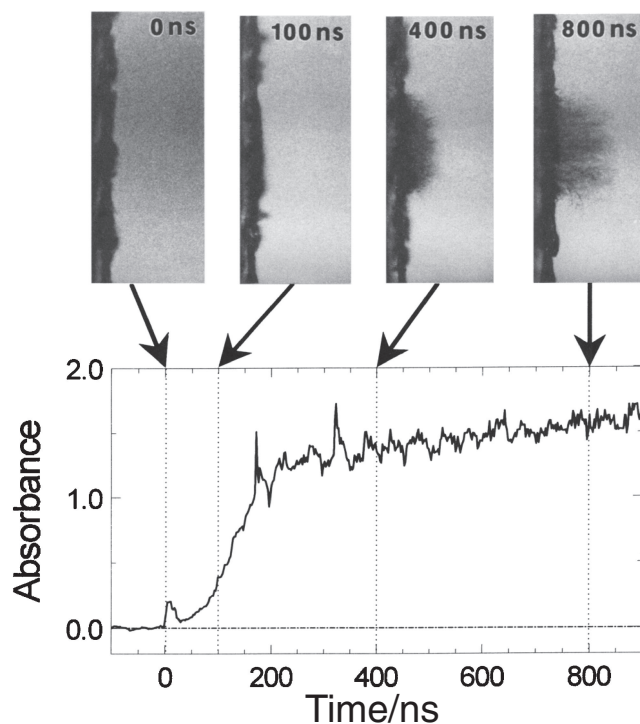


**Figure 1.** Comparisons between transient absorption at 360 nm and nanosecond photograph of poly(methyl methacrylate) film doped with 2.0 wt% biphenyl upon laser ablation. Laser fluence for absorption measurement and photograph is 670 and 600  $\text{mJ cm}^{-2}$ , respectively. This figure is reproduced from Figure 8 of Ref. 25. Copyright 2013 American Chemical Society.

ple the result on poly(methyl methacrylate) film doped with biphenyl is described here.<sup>25</sup> In Figure 1 absorbance at 360 nm and shadowgraph near the film surface are shown as a function of the delay time after 248 nm excitation. Here the materials ejection behavior was followed directly by nanosecond dynamic photography where an excimer laser (248 nm) and the second harmonic (532 nm) of nanosecond  $\text{Nd}^{3+}$ :YAG laser were used to induce ablation and to light a dye solution. The fluorescence of a methanol solution of rhodamine 101 worked as a flash lamp for nanosecond photography and its pulse width was 17 ns. Since morphological change upon intense excitation was induced at the small area of the sample film edge, observation was done under a microscope as shown in Figure 2.

As clearly seen in Figure 1, no appreciable ejection of fragmented debris was initially observed with the spatial resolution of a few tens of  $\mu\text{m}$ . In the delay time range of a few tens ns, the absorbance at 360 nm was detected even at the excitation of 360  $\text{mJ cm}^{-2}$  and ascribed to the triplet state ( $T_1$ ) of doped biphenyl molecule. This band rose rapidly and decayed fully before 50 ns, which is interpreted as  $T_1$ - $T_1$  annihilation due to its dense excitation condition. After that a very intense absorption increased, corresponding to ejection of the fragmented materials debris which was observed in the shadowgraphs. By introducing a streak camera into the setup in Figure 2, transient absorption spectra upon laser ablation were measured as one-shot event. The results are summarized in

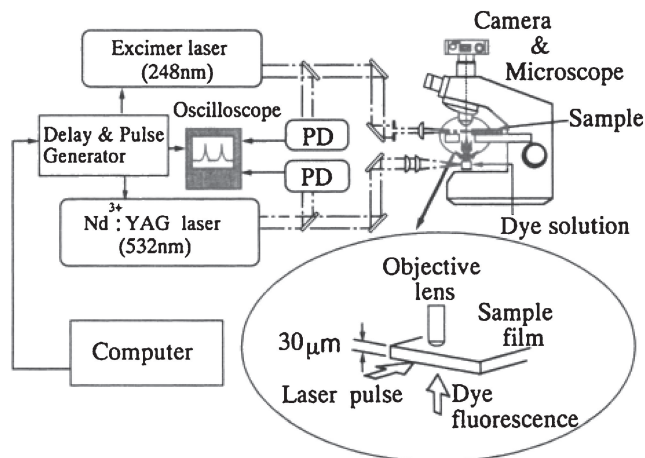


**Figure 2.** Schematic diagram of nanosecond photography. This figure is reproduced from Figure 1 of Ref. 25. Copyright 2013 American Chemical Society.

Figure 3. The transient absorption spectrum at early stage can be confirmed to be  $T_1$ , while the absorption band due to excited singlet state ( $S_1$ ) was not observed in the examined temporal and wavelength regions. At later delay time an extremely intense absorption tailing to the long wavelength emerged, which was ascribed to scattering due to ejected particles with size larger than the monitoring light wavelength.

Emission spectra were measured with a streak camera and summarized in Figure 4. The spectrum at early stage is assigned to biphenyl fluorescence, and its fluorescence decay dynamics is well correlated with the rise of the triplet absorption, namely, the singlet state is first generated and followed by intersystem crossing, involving  $S_1$ - $S_1$  and  $T_1$ - $T_1$  annihilation processes. Their decays under the present ablation condition are faster than the conventional monomolecular decays due to their mutual interactions. At later stages a very broad band overlapped with sharp peaks were detected, which should be ascribed to plasma emission and small radicals such as  $\text{CH}_2$ ,  $\text{C}_2$ , and so on, respectively. These emissions came to be prominent only at higher excitation intensity. Just above the ablation threshold, etching was observed without plasma emission. These results indicate that plasma and small radicals' emissions are ascribed to the subsequent processes and only  $S_1$  and  $T_1$  states are responsible to ablation, although plasma emission was quite frequently reported in the literatures on laser ablation of organic materials.<sup>50</sup> Therefore we consider that primary processes of laser ablation can be understood in the framework of Jablonski diagram.<sup>25</sup> This experimental result gave us an important remark that laser ablation of molecular materials can be studied as one of photochemistry researches. In the following we summarize two reports of our spectroscopic studies on laser heating of polymer films.

Laser heating dynamics of poly(methyl methacrylate) films doped with biphenyl or *p*-terphenyl was analyzed and photo-thermal laser ablation mechanism was considered to hold.<sup>38</sup> Temperature-dependent  $T_1$ - $T_1$  annihilation was analyzed in view of the thermally activated diffusion of the dopant species. The second-order rate constant for the  $T_1$  absorption was obtained at several temperatures under weak excitation (2–4

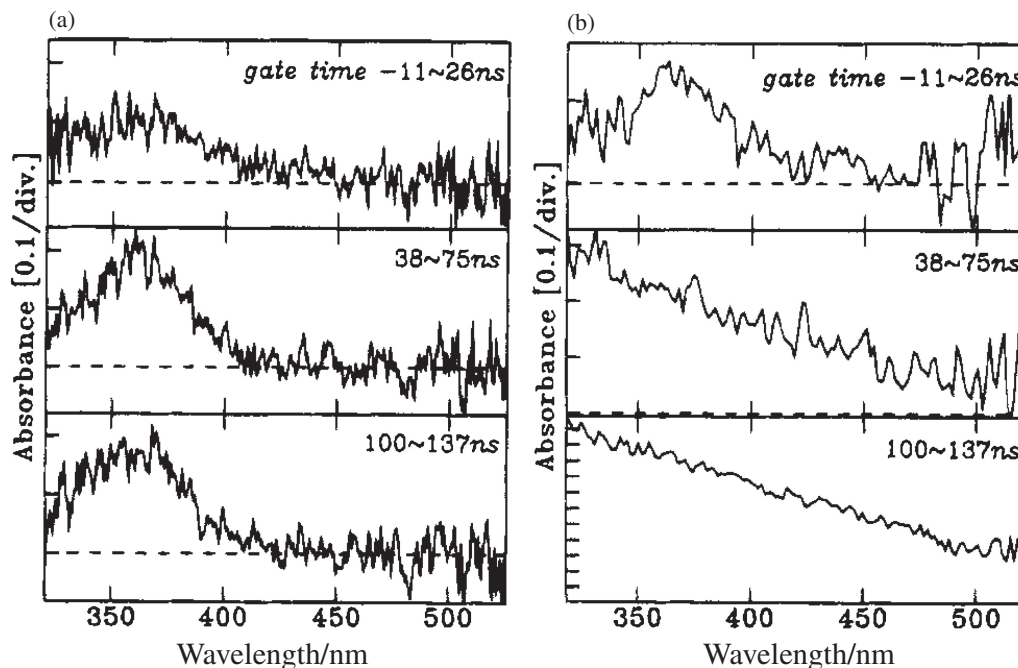


**Figure 3.** Time-resolved absorption spectra of poly(methyl methacrylate) film doped with 2.0 wt % biphenyl upon laser ablation. Laser fluence is (a) 30 and (b) 360  $\text{mJ cm}^{-2}$ . Gate time is given in the figure. This figure is reproduced from Figure 6 of Ref. 25. Copyright 2013 American Chemical Society.

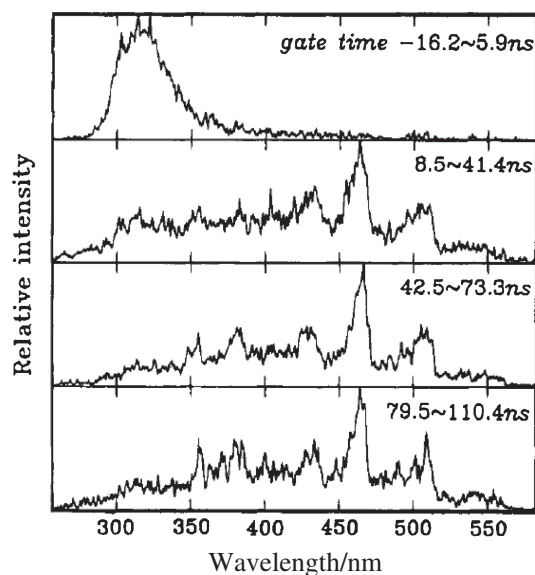


**Figure 4.** Time-resolved emission spectra of poly(methyl methacrylate) film doped with 2.0 wt % biphenyl upon laser ablation. Laser fluence is 3.7  $\text{J cm}^{-2}$ . This figure is reproduced from Figure 10 of Ref. 25. Copyright 2013 American Chemical Society.

$\text{mJ cm}^{-2}$ ), and its Arrhenius plot gave a straight line that was used to estimate the rate constant at higher temperatures for the simulation of  $T_1$ - $T_1$  annihilation. Under intense excitation (100–190  $\text{mJ cm}^{-2}$ ), the  $T_1$  states of both films decayed faster with an increase in laser fluence. The comparison of these observed  $T_1$  decays with simulated ones revealed that most of the observed photon energy, at least of 70%, is used to elevate temperature of the film. Also, the cooling of the polymer film,

mainly due to heat transfer to a quartz substrate, slows down the diffusion of the dopants and consequently the  $T_1$ - $T_1$  annihilation. The elevated temperature of the film remains almost constant at least for a few  $\mu\text{s}$  after excitation, during which fragmentation leading to etching may be induced.

Another kind of example is an poly(*N*-vinylcarbazole) film, where we could not find any appreciable transient absorption upon nanosecond laser ablation, but a tail of the ground state absorption was observed to be temporarily enhanced.<sup>19</sup> This behavior was interpreted that the excited singlet states disappeared efficiently due to their mutual interactions giving no appreciable transient species. By analyzing the absorption profiles at different laser fluence, the effective transient temperature below, at, and above the ablation thresholds was estimated. The temperature rise time was less than 50 ns, and the film was cooled down in a few  $\mu\text{s}$ . The temperature attained at the excitation intensity just below the ablation threshold (60  $\text{mJ cm}^{-2}$ ) was 260 °C and between decomposition temperatures (230–300 °C) of the film. Based on these results it was concluded that the photothermal decomposition mechanism is responsible to the ablation of this film.

**1.2 Cyclic Multiphoton Absorption as an Efficient Photothermal Conversion Process.** It is well known that simultaneous quantum mechanical and successive multiphoton absorption through some intermediate states are induced efficiently under intense laser excitation. The former takes place directly from the ground to excited states, while the latter consists of multistep absorptions via transient states which are usually excited singlet and triplet states. Under nanosecond laser ablation of the doped polymer films, the excitation power is so high that the concentration of the excited states of doped or chemically bonded molecules becomes often comparable to that of the ground state soon at the early stage during excitation

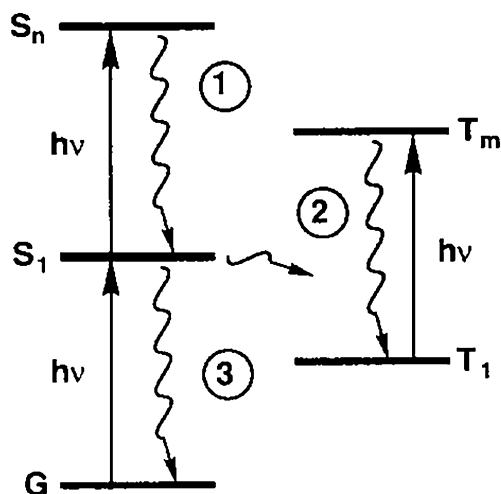


**Figure 5.** Possible mechanisms for cyclic multiphotonic absorption. ①  $S_n$ - $S_1$  mechanism; ②  $T_m$ - $T_1$  mechanism; ③  $S_1$ - $G$  mechanism. This figure is reproduced from Figure 2 of Ref. 22. Copyright 2013 Elsevier.

pulse. Thus the photon absorption by the intermediate state enough competes with that by the ground state. The key point here is that the higher excited ( $S_n$  or  $T_m$ ) state formed by successive absorption of  $S_1$  or  $T_1$  states relaxes rapidly to the original  $S_1$  or  $T_1$  state in the time scale of 10 ps and the latter state again can absorb successive photons. The absorption to and the relaxation from  $S_n$  or  $T_m$  take place rapidly so that they can repeat many times during nanosecond excitation, and as a result emitted intramolecular and lattice vibrational energy heats up to the surroundings enough to induce thermal decomposition. We named this process “cyclic multiphoton absorption” and concluded that this absorption results in photothermal ablation of dopant molecular systems.<sup>22</sup> The process is schematically given in Figure 5, along which the experimental results were summarized and discussed.

Polystyrene film doped with anthracene or anthracene- $d_{10}$  was ablated by 351 nm laser irradiation in a high-vacuum apparatus, and velocity distribution of ejected species were measured with a quadrupole mass spectrometer.<sup>20</sup> When the etching of the surface took place at irradiation energy of several hundreds  $\text{mJ cm}^{-2}$ , the detected species were mainly anthracene and styrene monomers. The result was analyzed by assuming a composite Maxwell-Boltzmann (MB) distribution with high temperature (several hundreds K) and low-temperature (250–300 K) MB components. It was considered that photon energy absorbed by anthracene is converted into thermal energy through rapid internal conversion in a polystyrene matrix, resulting in thermal decomposition of the polymer matrix. Moreover it was pointed out that 30 photons should be absorbed by individual molecules to prepare a melt polymer at 995 K, which is estimated translational temperature of anthracene obtained in the mass spectrometry measurement. It is interesting to understand how one anthracene molecule absorbs a few tens of photons during laser irradiation and why the photon energy is converted to heat without decomposing itself. This finding is well explained with “cyclic multiphoton absorption” process which we described above. As the first

excited singlet state of anthracene absorbs photon and the formed higher excited state quickly relaxes to the first excited state, emitting vibrational energy, and the recovered excited state absorbs photons again. Thus anthracene is regarded to be a “molecular converter” of absorbed photon energy into the surrounding heat energy.

To confirm this cyclic multiphoton absorption process in more detail, temporal profile of the dopant fluorescence was measured and compared to the computational results based on cyclic multiphoton absorption in the ground state,  $S_1$ , or  $T_1$  state.<sup>22</sup> It was revealed that simulation based on the cyclic multiphoton absorption mechanism through  $S_n$ - $S_1$  and  $T_m$ - $T_1$  relaxation well reproduced the fluorescence rise and decay curves upon the laser ablation of the polystyrene film doped with 0.1 M anthracene. Moreover calculated temperature based on the mechanism through  $T_m$ - $T_1$  transition agrees closely with the mean temperature of ejected anthracene and styrene obtained by mass spectroscopy. Thus we concluded that the cyclic multiphotonic absorption mechanism through  $T_m$ - $T_1$  relaxation is most probable in the anthracene-doped polystyrene film.

The 248 nm ablation of pyrene-doped poly(methyl methacrylate) film was investigated with much attention to the dynamics of pyrene transient species under intense excitation.<sup>27</sup> It was shown that pyrene is stable even when it absorbs more than several photons during the laser pulse, which is again well explained in terms of cyclic multiphoton absorption process. This means that the photodecomposition of a dopant is not involved, while multiphoton absorption partly may lead to ionization giving pyrene cation. This is reasonable, since only ionization can compete with fast vibrational relaxation taking place with 10 ps and decomposition reaction needs longer time scale. Indeed the excited singlet, triplet, and cation states of pyrene were detected within and after the laser pulse by nanosecond emission and absorption spectroscopy. The broadening and red shift of the fluorescence of pyrene at 440  $\text{mJ cm}^{-2}$  mean that not only pyrene but also the polymer film are heated and become hot, which supports photothermal ablation of pyrene-doped poly(methyl methacrylate) film. The triplet and cation states of pyrene are produced through the excited singlet state of pyrene, contributing to cyclic multiphotonic absorption as intermediate states. It was also shown that the temperature elevation due to photoabsorption facilitates the excited singlet-singlet and triplet-triplet annihilation processes and also the recombination of the cation and electron or anion.

Dynamics of  $N,N,N',N'$ -tetramethyl- $p$ -phenylenediamine in poly(methyl methacrylate) was also studied spectroscopically under 248 nm ablation condition.<sup>31</sup> The spectral behavior was well interpreted in terms of the dynamics of the excited singlet and triplet states and a cation of the doped amine. The decay processes of all the detected transient species became fast with an increase in the laser fluence. It was directly shown that one dopant molecule can absorb 8 photons during the nanosecond laser pulse at the 248 nm ablation threshold. These results are well explained again by the cyclic multiphoton absorption mechanism where the transient species of the dopant work as respective absorbers of the laser photons. The mechanism is consistent with the fact that the excited state energy level of

ion radicals is usually low and small energy gap between the excited and ground states of ions gives short lifetime to ion radical. Namely the ion radical can repeat absorption and relaxation efficiently.

The 248 nm laser ablation dynamics of poly(methyl methacrylate) (PMMA) film doped with 5-diazo meldrum's acid was investigated as we expected that the dopant is easily decomposed and induces photochemical ablation.<sup>26</sup> We confirmed that the photodecomposition of the dopant itself has little or no effect on laser ablation as it did not damage the films, while temperature elevation through the cyclic multiphotonic absorption by the generated ketene eventually led to laser ablation. Namely the ketene which is formed through photodecomposition of 5-diazo meldrum's acid undergoes repetitive absorption and relaxation during the excitation pulse as the excited state lifetime of ketene is enough short. Thus we consider that cyclic multiphoton absorption process is also applicable to 5-diazo meldrum's acid dopant and its photochemical transient species is responsible to repetitive absorption. It is concluded that cyclic multiphotonic absorption process holds generally for laser ablation of various doped polymer films.

### 1.3 Expansion and Contraction Dynamics of Polymer Films by Nanosecond Time-Resolved Interferometry.

Ablation is a nonlinear photochemical phenomenon with respect to laser fluence and its resultant etching is observed only when the fluence is higher than the threshold value. Even below the threshold, however, a number of photons are absorbed by polymer films, so that heating effect is considered to be appreciable. In other words the film should be expanded by heating and then cooled down leading to shrinking. If this expansion and contraction are monitored by time-resolved measurement, dynamic morphology change will be made clear. In 1994 we first developed nanosecond interferometry and succeeded in observing directly expansion/contraction dynamics of polymer films.<sup>24</sup> This system is in principle based on a Michelson-type interferometer whose schematic diagram is shown in Figure 6. An excimer laser or a tunable OPO system was used as an excitation light source, while the 2nd harmonic pulse (532 nm, 14 fwhm, 10 ns) of the Q-switched Nd<sup>3+</sup>:YAG laser was used as a probe light. The excitation pulse was focused onto a sample surface at a slightly tilted angle, while the probe beam was divided into two; one for the sample surface and the other for a reference quartz glass with respective normal angles. By combining two beams reflected from the sample surface and the quartz glass, interference patterns were formed, which was detected by a CCD camera. The original of the delay time ( $\Delta t$ ) was defined as the time when both peaks of excitation and probe pulses arrive at the polymer surface simultaneously. In the experiment, a fringe shift to the left or right corresponds to an expansion or etching depending on optical condition. One fringe spacing is a half wavelength of the probe laser, that is, 266 nm, and one twentieth can be resolved by our CCD camera. Consequently the surface displacement (expansion or contraction) can be obtained with resolution of 13 nm, while time resolution is 10 ns which is determined by the probe light pulse. We call this system nanometer-nanosecond interferometry and applied to various polymer films.

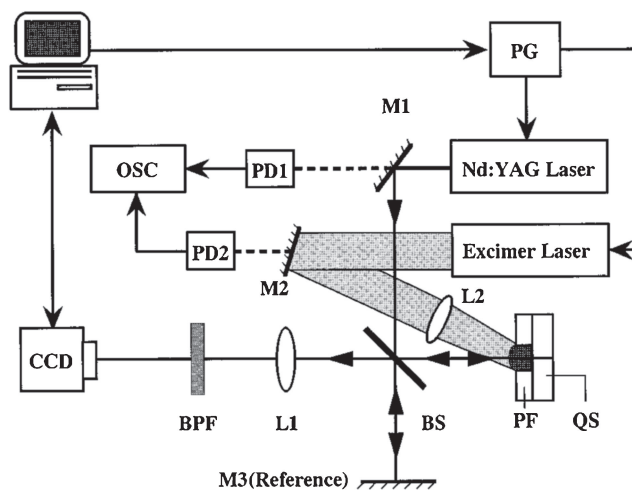


**Figure 6.** A schematic diagram of a nanosecond time-resolved Michelson interferometer; PF, a polymer film; QS, a quartz substrate; M1–M2, mirrors; L1–L2, lenses; BS, a beam splitter; PG, a pulse delay generator; OSC, a sampling oscilloscope; PD1–PD2, photodiodes; CCD, a video camera; BPF, a band pass filter. This figure is reproduced from Figure 1 of Ref. 24. Copyright 2013 American Institute of Physics.

Surface morphological change dynamics below and/or above the ablation threshold of various polymer films was examined systematically, whose representative images of polyimide film are shown in Figure 7.<sup>48</sup> The fringe shift toward left side corresponds to expansion under the experimental condition. Below the ablation threshold polymer film expanded immediately after excitation and then slowly contracted to the original thickness, just as etching started just after excitation above the ablation threshold. Thus, transient expansion and etching dynamics can be elucidated obtained by analyzing the nanosecond time-resolved interferometric images.

A comparative interferometric study of poly(methyl methacrylate) and poly(methyl acrylate) gave us new information of glass-rubber transition dynamics, which was obtained for their films doped with pyrene.<sup>41</sup> At 150 mJ cm<sup>-2</sup> of the 248 nm excitation, which is below the ablation threshold, polymer film of ca. 2  $\mu$ m thickness underwent rapid expansion of about 250 nm and the following slow contraction, resulting in no permanent etching on the surface. Shrinking behavior of irradiated PMMA films on two different kinds of substrates, quartz and undoped commercial PMMA plate, was compared with each other. The expansion of the PMMA film on the quartz plate disappeared after 20 ms, while PMMA film on the undoped PMMA plate showed very slow contraction, that is, the expansion disappeared after a few seconds. This result indicated that contraction dynamics of the PMMA film affected by the substrate. Since the thermal diffusivity of a PMMA substrate is lower than that of quartz one, which supports our proposal that the thermal process has a major role in the transient expansion of PMMA films upon pulsed laser irradiation.

Based on photothermal mechanism, we extended systematic study on pyrene-doped PMMA and related films. Fluence dependence of the maximum expansion amplitude of PMMA and PMA films doped with 2 wt % pyrene was investigated and

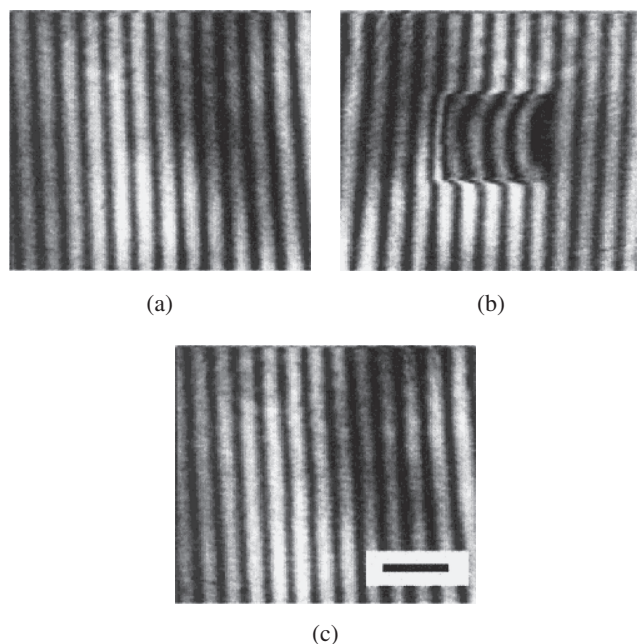


**Figure 7.** Nanosecond time-resolved interferometric images of polyimide film on a wedged quartz plate at the fluence of  $130 \text{ mJ cm}^{-2}$  below the ablation threshold, which was obtained with the surface configuration. The excitation wavelength is 351 nm. The fringe shift to the left represents an expansion. Delay time is (a) before excitation, (b) 24 ns, and (c) enough after excitation. The black bar in panel (c) indicates 1 mm in the image. This figure is reproduced from Figure 1 of Ref. 48. Copyright 2013 American Chemical Society.

obtained result is plotted in Figure 8.<sup>41</sup> Around  $65 \text{ mJ cm}^{-2}$ , a knick point was observed for PMMA film and the slope increased by a factor of about 4.2, whereas the PMA film did not alter the slope. It is worth noting that only PMMA film shows the discontinuous fluence dependence. Surface temperature of PMMA at the knick point was estimated to be about 410 K, which is a little higher than glass–rubber transition temperature ( $T_g$ ) of PMMA; 378 K. We estimated the temperature by assuming that the Lambert–Beer law holds and all absorbed photons are converted to heat. The absorbance of films obtained by conventional absorption spectrometry, while the thickness of the films measured by a depth profiler were used for the estimation. Although this estimation was later deemed too rough, it was enough to consider that the discontinuous fluence dependence of the expansion amplitude was due to the glass–rubber phase transition of PMMA. Thermal expansion coefficient of the PMMA film increased when temperature exceeds  $T_g$ , which explains the slope change. On the other hand, PMA is in the rubbery state at room temperature even before excitation, so that such a knick point was not observed.

In addition to expansion/contraction dynamics, etching behavior of a neat PMMA film was also investigated by 248 nm excitation under higher excitation condition and directly measured by nanosecond interferometry.<sup>34</sup> Above the ablation threshold ( $1400 \text{ mJ cm}^{-2}$ ), the film expands during excitation, and after 25% expansion of the thickness, we could not get a clear fringe pattern of the interference images of the irradiated

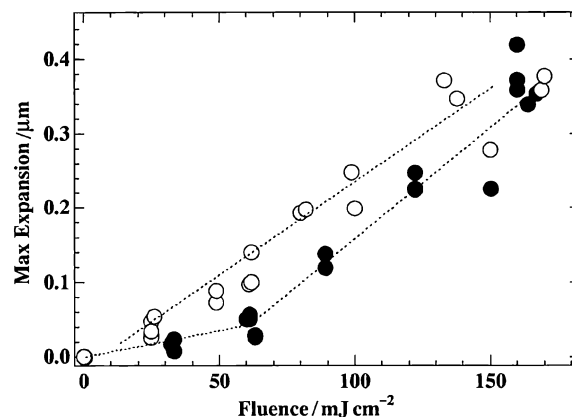


**Figure 8.** Fluence dependence of the maximum expansion of PMMA (●) and PMA (○) films below the ablation threshold ( $180$  and  $330 \text{ mJ cm}^{-2}$ , respectively). Both films are doped with 2 wt% pyrene. This figure is reproduced from Figure 3 of Ref. 41. Copyright 2013 American Chemical Society.

area. This is because interference images became dark, which is eventually ascribed to ablated fragments. Below the threshold, the expansion rate is still high (a few  $\text{nm ns}^{-1}$ ), and permanent swelling is observed after transient expansion and succeeding contraction. Permanent swelling was not observed by decreasing the laser fluence below  $800 \text{ mJ cm}^{-2}$ , which was called swelling threshold. The expansion amplitude as a function of laser fluence indicates that the neat PMMA film also undergoes phase transition from glass to rubber, which takes place at a fluence higher than  $450 \text{ mJ cm}^{-2}$ .

In further low fluence range where the transition is not involved, neat poly(methyl methacrylate) showed a novel expansion and contraction behavior as given in Figure 9.<sup>33</sup> The morphological change of several tens nm occurred repetitively in a few hundreds ns time range, and then the film shrank to the original thickness. This behavior was not observed for other polymers such as polystyrene, triazenopolymer, nitrocellulose, and so on. In glassy region below the phase transition temperature, the film behaves like a rigid solid and quick laser heating results in a rapid expansion and its overshooting may lead to the oscillatory behavior. On the other hand, a large slippage of polymer chains upon heating results in the glass–rubber transition.

These photothermal behaviors are probably ascribed to the differences in polymer chain entanglement in the given states. The entanglement was also reflected in cooling dynamics of laser-heated polymer film. We studied molecular weight dependent surface morphological changes of polystyrene film after 248 nm excimer laser irradiation.<sup>36</sup> In the case of low molecular weights ( $3.0 \times 10^3$  and  $5.0 \times 10^3$ ), the surface contracts exponentially. In the case of high molecular weight ( $1.0 \times 10^6$ ), however, two different contraction processes were observed, that is, a major contraction and a minor tail. The thermal diffusion coefficients acquired experimentally from the contraction of polymers with both high and low molecular weights are almost the same as the value in the literature, which indicates thermal diffusion is dominant for the major contraction. On the other hand the minor tail was observed only

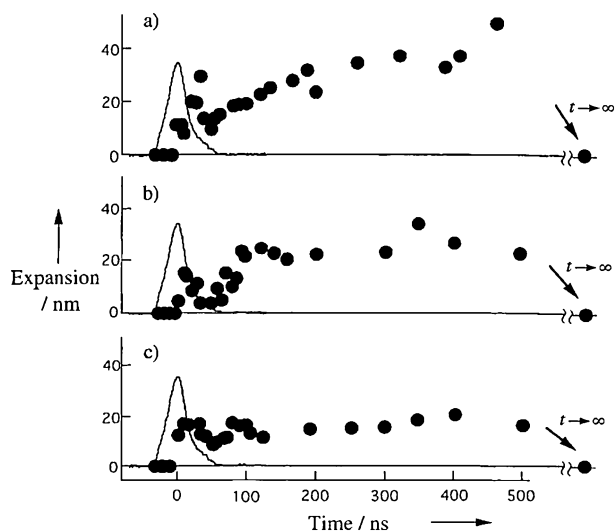


**Figure 9.** Expansion and contraction dynamics of PMMA at fluence of (a) 400, (b) 300, and (c) 250  $\text{mJ cm}^{-2}$ . A solid curve represents an excitation pulse shape. This figure is reproduced from Figure 3 of Ref. 33. Copyright 2013 Wiley-VCH Verlag.

when the molecular weight is larger than that corresponding to characteristic length, so that it was considered that the tail shows the effect of the entanglements.

**1.4 Nanosecond Laser Ablation of Photodecomposable Polymer Films.** Photothermal ablation is induced by local and transient temperature elevation due to efficient conversion of excitation energy to molecular and eventually lattice vibrations. If bond cleavage of the excited states forming small gaseous molecules is enough fast to compete with electronic and vibrational relaxations, photochemical ablation is realized. Some polymers having photodecomposable bonds or chromophores, which are specially designed, show this ablation, whose representative examples are summarized below. It is clear that the time-resolved interferometry is very useful to analyze laser-induced reaction of polymer films, particularly to discriminate between photothermal and photochemical ablation.

**1.4.1 Nitrocellulose Film:** Laser-induced decomposition and accompanying ablation dynamics of a reactive nitrocellulose film was investigated by doping a copper-phthalocyanine derivative as a light absorber.<sup>51</sup> Their chemical structures are given in Figure 10. While nitrocellulose does not absorb 351 nm XeF excimer laser pulse, the film heated instantaneously via rapid photothermal conversion in the doped copper-phthalocyanine derivative molecule. This rapid heating process in nanosecond excitation is well elucidated spectroscopically for phthalocyanine solid film.<sup>52</sup> Below the ablation threshold, thermal expansion and contraction processes of nitrocellulose film were directly followed by the nanosecond-nanometer interferometry. The dynamic interferometric observation is summarized in Figure 11. Above the ablation threshold, the expansion of the film was started during the excimer laser irradiation, and then explosive decomposition was initiated, continuing for a few hundreds ns after the excitation. Temperature elevation caused by the excimer laser irradiation results in an exothermic decomposition of nitrocellulose,

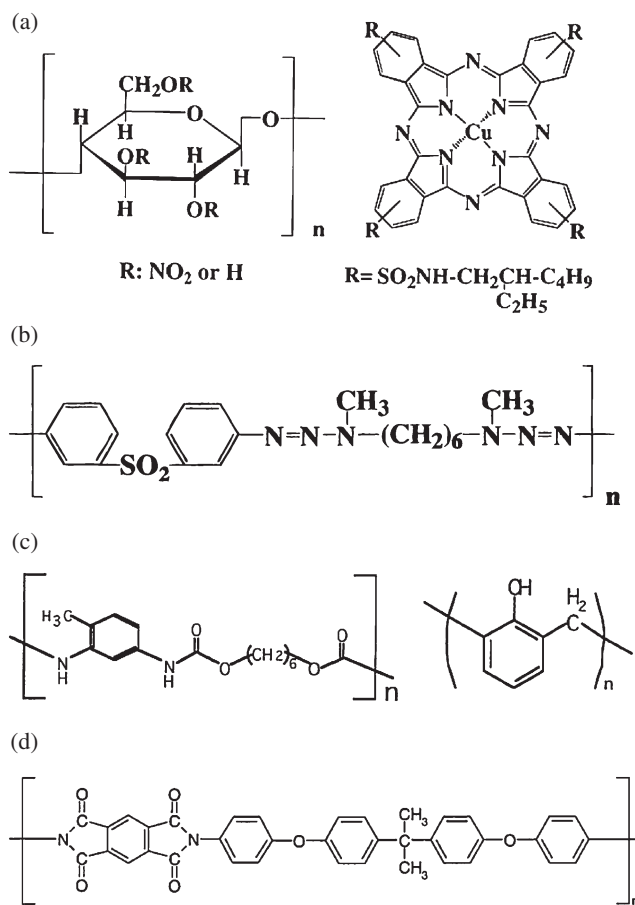


**Figure 10.** Chemical structures of (a) nitrocellulose (left) and savinyl blue (right), (b) triazeno polymer, (c) polyurethane (left) and phenol resin (right), and (d) polyimide.

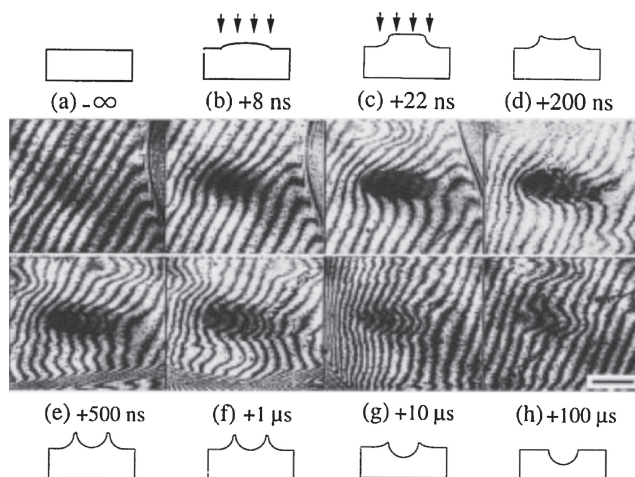


**Figure 11.** Nanosecond interferometric images of nitrocellulose/savinyl blue/polyurethane film at  $110 \text{ mJ cm}^{-2}$ . The bar in the figure represents 1 mm. Schematic illustration of expansion and etching at each stage is given above or below the images. This figure is partly reproduced from Figure 6 of Ref. 51. Copyright 2013 American Chemical Society.

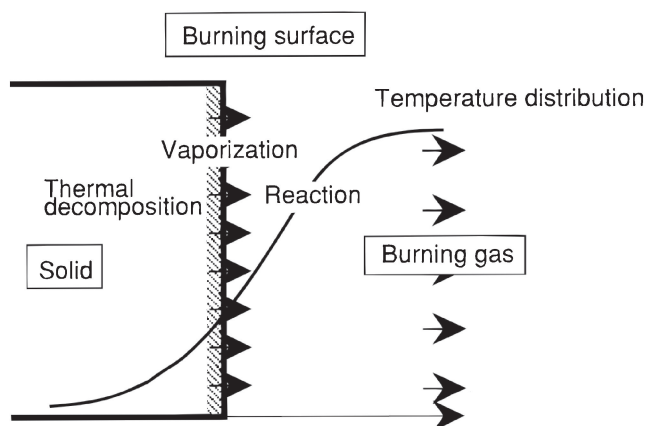


**Figure 12.** Illustration for combustion of materials: Solid surface is decomposed and vaporized, and the surface draws back. This figure is reproduced from Chart 2 of Ref. 51. Copyright 2013 American Chemical Society.

leading to a further heating of the film. Consequently self-acceleration of the reaction is enhanced and an explosive self-sustaining decomposition is induced after reaching the explosive decomposition condition. This is indeed characteristic of this film which is brought about by intense laser irradiation and schematically illustrated in Figure 12.

**1.4.2 Toriazene Polymer Film:** The dynamic behavior of photoetching process of a photosensitive triazenopolymer film was studied during and after 351 nm laser irradiation the nanosecond–nanometer interferometry.<sup>44</sup> Its chemical structure is given in Figure 10. At a fluence of  $250 \text{ mJ cm}^{-2}$ , a slight swelling of the film and darkening of the irradiated surface was initially observed, and then the etching process of the film was brought about around the peak time of the excitation laser pulse. The etching proceeded during laser irradiation and stopped almost at the end of the excimer laser pulse. On the other hand, at a fluence of  $60 \text{ mJ cm}^{-2}$ , the etching started from nearly the end of the excimer laser pulse and the etching process continued until 140 ns. When the laser fluence is high enough, photodecomposition occurs densely leading to sudden ablation, so that thermal degradation cannot be observed. On the other hand, at  $60 \text{ mJ cm}^{-2}$  the thermal process was successfully measured as photodecomposition is stopped. Since the decomposition of the triazenopolymer is an exothermic reaction, it is considered that photodecomposition of the polymer results in the temperature elevation, causing thermal degradation.

**1.4.3 Polyurethane Film:** A polyurethane sample film was prepared by adding phenol resin as a structural stabilizer and dynamics of laser-induced morphological change was investigated upon 248 nm excitation.<sup>35</sup> Chemical structures are shown in Figure 10. The ablation threshold by 248 nm excitation was determined to be  $40 \text{ mJ cm}^{-2}$ . Below the ablation threshold an expansion forms a bump and followed by rapid contraction, that is, expansion disappeared at about  $1 \mu\text{s}$ . Above the ablation threshold interferometric images were not disturbed by the decomposed products, which indicates that the film was decomposed rapidly into debris, fragments, aggregates, and so on. They should be smaller than visible light

wavelength, as images are clear and not disturbed. Indeed no appreciable debris was left. It is also noticeable that transient expansion was not observed. At the fluence of  $310 \text{ mJ cm}^{-2}$ , etching proceeds fast during the initial half of the excitation laser pulse, but stopped at the late stage of the pulse. The morphological behavior is quite different from that of photo-thermal expansion and contraction dynamics characteristic of PMMA. Hence it is considered that laser ablation is induced photochemically.

**1.4.4 Polyimide Film:** Intense excimer laser excitation of polyimide film gives transient expansion and the following contraction, permanent swelling, and ablation, depending on excitation wavelength.<sup>48</sup> The chemical structure of the polymer is given in Figure 10. Ablation by 248 nm excitation takes place only during the excitation laser pulse and no debris was observed, while ablation by 351 nm excitation is brought about after expansion. Permanent swelling was observed only for 351 nm excitation. Expansion and contraction dynamics at low fluence of 351 nm excitation is consistent with the simulation of temperature rise. This means that photothermal mechanism surely holds for the 351 nm excitation. At 248 nm excitation, on the other hand, a hump in expansion and contraction profile becomes clear. We explained this dynamics in terms of photochemical formation and recombination/leakage of decomposed small molecules. On the basis of the morphological dynamics, we considered that photochemical and photothermal mechanisms mostly explain the results obtained by 248 and 351 nm excitation, respectively.

## 2. Femtosecond Laser Ablation Dynamics and Mechanism

Femtosecond laser ablation has been receiving much attention as a fabrication method since the etched surface is generally smoother compared to nanosecond ablation. This suggests that the ablation takes place involving less thermal effect. The advantages and disadvantages had been discussed mainly based on observation of etched surface morphology, but information on ablation dynamics by applying time-resolved spectroscopy and imaging was and is still limited. Plasma emission upon ablation was reported frequently, which is ascribed to the fact that emission spectral measurement is relatively simple and easy compared to UV–visible absorption, IR absorption, and Raman spectroscopy. As a consequence it is roughly recognized that femtosecond ablation is due to plasma formation. By studying dynamics and mechanism of nanosecond laser ablation as summarized above, however, we had come to the consideration that molecular photophysical and photochemical primary processes should hold for femtosecond ablation of organic materials and be just modified because of very intense laser excitation. We expected that similar spectroscopic and imaging approaches which we had applied to nanosecond ablation studies would be useful for elucidating femtosecond ablation dynamics and mechanism. Furthermore it was reasonable to assume that optical measurements in early time range are easier than in nanosecond one as materials ejection is always delayed compared to photochemical and photophysical processes. Thus our strategy was to apply various time-resolved measurement methods for elucidating ablation the phenomena depending on femtosecond, nanosecond,  $\mu\text{s}$ , and later time ranges, which is schematically shown in Figure 13.

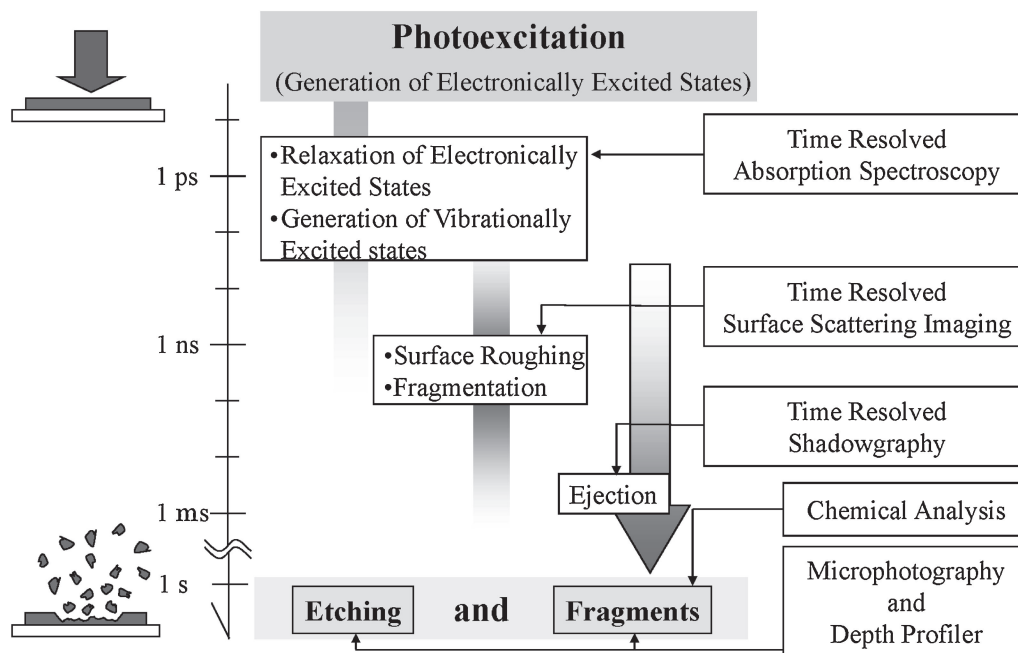


**Figure 13.** Our strategy for elucidating laser ablation by direct measurements with time-resolved spectroscopy and imaging.

**2.1 Surface Roughening Dynamics by Femtosecond Surface Light Scattering Imaging.** In the framework of Jablonski diagram, photoexcitation energy generates excited singlet and triplet states which are followed by energy, electron, and proton, or hydrogen atom transfers. These processes can be directly probed by emission and absorption spectroscopic methods. The plasma state which is sometimes considered to be a key step for ablation is also identified by its broad emission in the visible region. On the other hand, ablation include various phenomena such as melting, expansion, vaporization, gas bubbling, fragmentation, nm and  $\mu\text{m}$  particle formation, and so on are monitored by time-resolved imaging methods. Time-resolved photography which is called shadowgraphy is generally applied, but its spatial detection limit is of course larger than the wavelength, namely, a few hundreds nm. Expansion and contraction of polymer films can be followed with 10 ns and 10 nm resolutions by our interferometry as described above, however, the moving polymer surface should be enough flat over the lateral direction of a few mm. It was not easy to follow initial dynamics of fragmentation as far as we knew. When we started femtosecond ablation study, it was considered that nanometer surface morphological change is one of the early events following electronic excitation and relaxation in laser ablation. This surface dynamics became monitored by developing time-resolved surface light scattering imaging, whose advantage was demonstrated first for laser ablation of liquid benzene<sup>53</sup> and amorphous copper-phthalocyanine.<sup>54</sup> Here we summarize experimental setup, example, and how to get information on surface morphology change by showing data on copper-phthalocyanine films.

The schematic diagram of our surface light scattering imaging system is given Figure 14. The 800 nm light of a regenerated amplified femtosecond Ti:sapphire laser was divided into two pulses; one was used as an excitation light and the other for generating femtosecond white light continuum

extending from 400 to 1000 nm. The excitation and probe pulses are almost normally incident on the film, while the scattered light from the latter was detected at an angle of  $50 \pm 18^\circ$ , and recorded with a CCD camera. The observation wavelength region adopted was  $535 \pm 17$  nm. The origin of the time axis was determined by measuring transient absorption spectra of amorphous copper-phthalocyanine films, which measurement is described later. All the measurements were done for a fresh surface of the film.

As typical examples, the scattering images of multicrystalline copper-phthalocyanine film upon laser ablation are shown in Figure 15. At  $62 \text{ mJ cm}^{-2}$ , which is larger than the threshold fluence by 1.5 times, the surface scattering from the central part of the irradiated area was observed, which is consistent with the Gaussian-like laser beam profile. It is worth noting that no appreciable change was detected in the picosecond time region, while its intensity grew in a few ns. In general two possible origins are examined; one is Rayleigh scattering due to vaporized copper-phthalocyanine and/or its nanoparticles, and the other is ascribed to nonspecular reflection from the roughened surface. As Rayleigh light scattering is usually very weak, it is expected that the diffusely reflected light from the roughened surface gives the present scattering images. The scattered intensity was practically correlated to the roughness of the surface and we evaluated quantitatively the increase in the roughness. Namely we prepared some copper-phthalocyanine films with different roughness by applying spin-coating and casting, and their surface morphology was evaluated by AFM observation and the average surface roughness was obtained. The same films were probed by the femtosecond surface light scattering imaging system without femtosecond excitation. Then we could get a correlation curve between the average surface roughness and the scattering intensity. This is our new approach which has never been reported as far as we know. The evolution of the surface roughness of microcrystal-

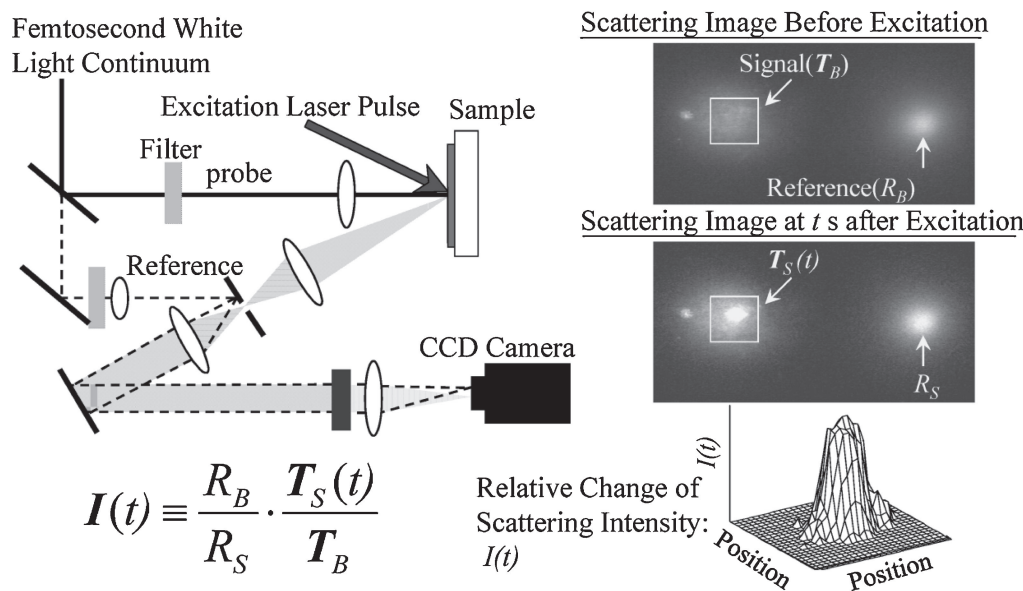


Figure 14. Femtosecond surface light scattering imaging system and sample images.

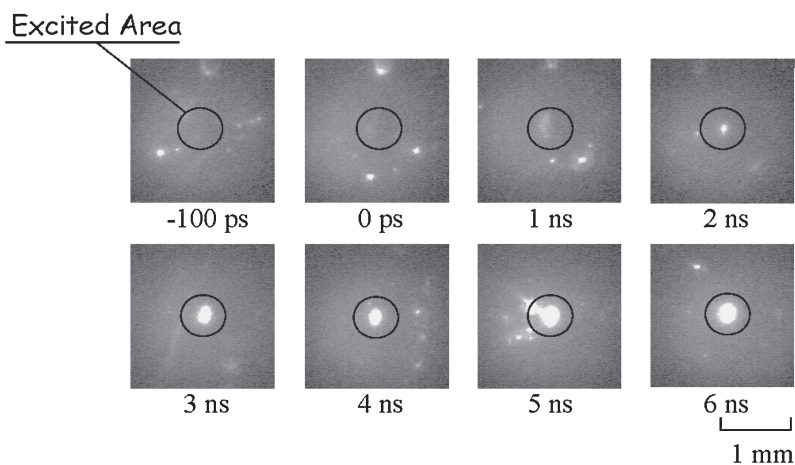


Figure 15. Sequential surface light scattering imaging of phthalocyanine film as a function of delay time upon laser ablation. Bright spots outside the excited area are due to protrusions during film casting.

line copper-phthalocyanine was estimated as in Figure 16. It is extremely interesting to see that the surface roughening is brought about in ns and even tens ns, although the excitation was done by the 100 fs pulse.<sup>55,56</sup> This induction time is very meaningful for elucidating ablation mechanism as discussed below.

### 2.2 Time-Resolved Electronic Absorption Spectroscopy.

As shown in nanosecond laser ablation of doped poly(methyl methacrylate) films, initially optical conditions of the irradiated sample films are not much disturbed and optically clear, which is fit to absorption spectroscopy. Indeed we succeeded in measuring femtosecond transient absorption spectra of copper-phthalocyanine film upon intense excitation.<sup>55-57</sup> Typical spectra below and above the threshold are given in Figure 17. A broad positive band was observed around 520 nm and assigned to electronically excited state of copper-phthalocyanine, namely exciton in this case, while the negative peaks at late delay times are due to spectral change of the ground state absorption. The exciton decay depended upon excitation

intensity and was in the time domain of 10 ps, and replaced by the absorption having negative and positive peaks. It was indeed a turning point of our research when we found the similarity between the spectral at the late stage and the temperature difference spectra. We set the microcrystalline film at the sample holder for the femtosecond absorption spectral measurement and measured absorption spectra without excitation, but by changing the sample temperature. Thus we obtained the temperature difference spectra of the ground state by the femtosecond setup. The transient spectrum observed at a few ns delay time and the temperature difference spectrum are similar to each other, except in the wavelength region above 700 nm. In the latter region some dimer peak is located, and its contribution to the exciton and ground state hot bands are considered not to be identical. Neglecting this contribution, we could estimate the local and transient temperature by comparing the transient spectra with temperature difference spectra. At the fluence of  $100 \text{ mJ cm}^{-2}$ , temperature elevation was estimated to be 250 K and at the ablation threshold the temperature

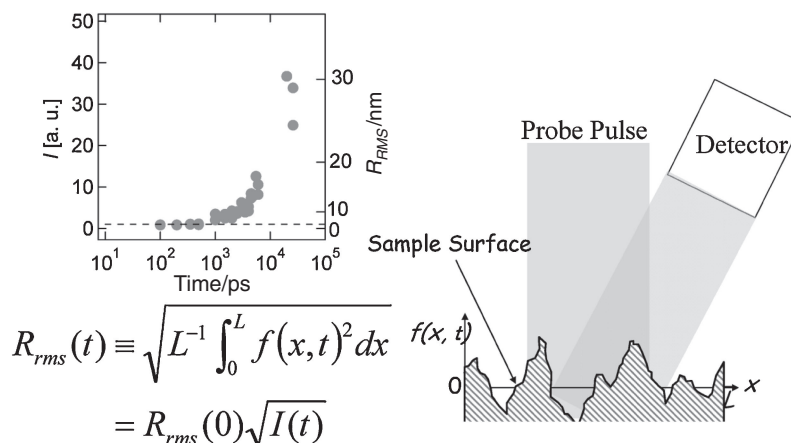


**Figure 16.** Temporal evolution of surface roughening ( $R_{rms}$ ) of phthalocyanine film upon laser ablation analyzed by femtosecond surface light scattering imaging.

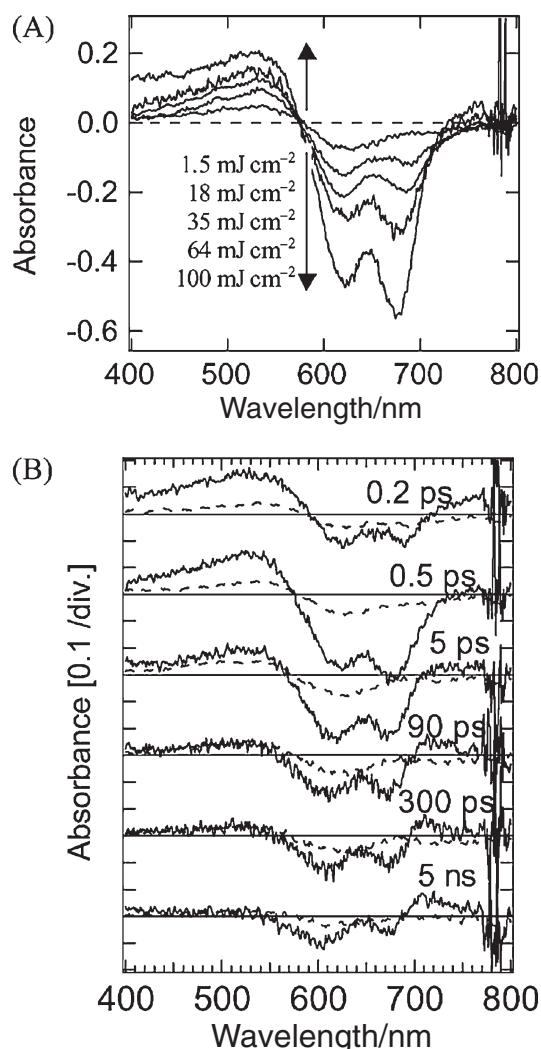


**Figure 17.** Femtosecond pump-fs probe absorption spectra at 0.5 ps by changing laser fluence (A) and at the laser fluence of 64 (solid line) and 1.5 mJ cm<sup>-2</sup> (broken line) (B). Delay times are given in the figure. This figure is reproduced from Figure 6 of Ref. 57. Copyright 2013 Elsevier.

jump was 100 K. These values of temperature are too low to induce melting, decomposition, and rapid vaporization, but it should be noticed that the temperature elevation speed is extremely fast; 1013 K s<sup>-1</sup>.

**2.3 Transient Pressure Mechanism for Femtosecond Laser Ablation.** On the basis of femtosecond imaging and transient absorption spectral measurements, it was concluded under the examined conditions that electronic excitation energy is converted to molecular and lattice vibrational energies in about 20 ps, and the attained temperature is not high at the ablation threshold (room temperature + 100 K). It is known that the sublimation starts at 380 °C and decomposition reaction is brought about at 550 °C. Thus, photothermal mechanism cannot explain the present femtosecond laser ablation. We noticed that we should pay our attention to the time scale of photothermal conversion of 20 ps which was clarified directly by transient absorption spectroscopy. On the other hand, it is described above that nanometer surface morphological changes were not observed until 1 ns after the 100 fs excitation. Namely there is some time lag between the local and transient heating (ca. 20 ps) and the morphological change (ca. 1 ns) as illustrated in Figure 18, which is very important to understand the femtosecond laser ablation mechanism.<sup>56</sup> During this lag time, vigorous molecular motions lead to pressure increase in every direction so that a mechanical stress should be accumulated in the film.<sup>54</sup> Thermal conduction is relatively slow in organic materials, so that the time lag is kept to be appreciable. Since the surrounding of the excited area is cold and the bottom is a quartz substrate, the stress can be released only by splitting the irradiated films into two layers. Here an example is multicrystalline copper-phthalocyanine film which is composed of nanocrystals where they associate with each other due to van der Waals force. Consequently, the upper layer was ejected while the lower layer remained on the substrate. Thus the mechanism is called “transient pressure mechanism,” which is consistent with molecular dynamics simulation on laser ablation by Zhigilei and Garrison.<sup>58</sup>

This mechanism is exclusively applied to femtosecond ablation and does not hold for nanosecond one. During the nanosecond excitation mutual interactions between excitons take place and enhance molecular and lattice vibrations, and

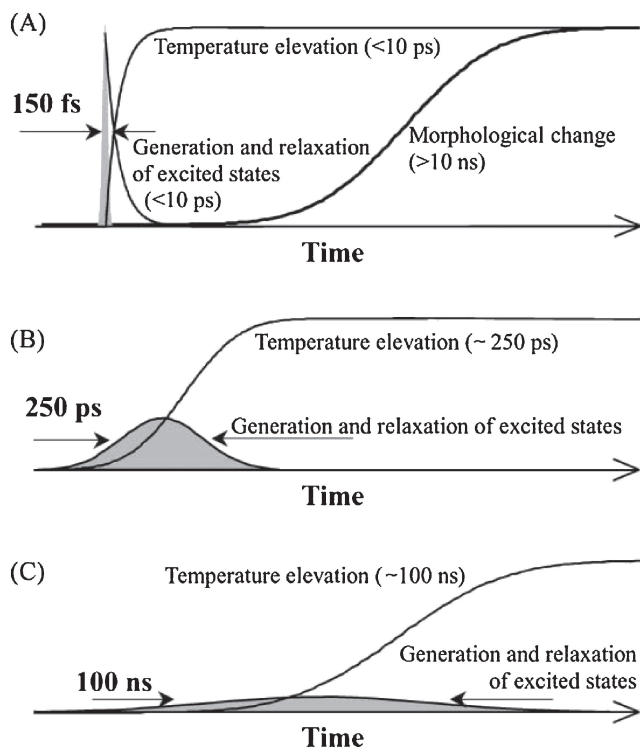


**Figure 18.** The temporal evolution of photothermal processes and morphological change when (A) fs, (B) ps, and (C) ns pulses were applied as the excitation pulse. This figure is reproduced from Figure 12 of Ref. 57. Copyright 2013 Elsevier.

their motions are efficiently transferred to the surroundings in this time range. Namely some gradient of molecular and lattice vibrations from the irradiated area to the outside is formed and transient pressure is not raised. Therefore photothermal heating mechanism is applicable, which was confirmed directly just by replacing the 100 fs pulse of the Ti:sapphire laser to 100 ns pulse of the same laser for the same copper-phthalocyanine films.<sup>56</sup> Without any doubt the nanosecond ablation mechanism of the copper-phthalocyanine film is consistent with the mechanism of nanosecond mechanism discussed above for polymer films.

### 3. Laser Ablation in Solution for Nanoparticle Preparation

Laser ablation has been applied for fabrication of metals, silicone, and related semiconductors materials, and their fabricated structures still possess original properties.<sup>2</sup> On the other hand organic materials, cells, tissues, and so on are considered to involve chemical decomposition upon ablation, resulting in large changes not only in physical and chemical properties but also in morphology. Our mechanistic studies described above, however, indicate that conventional photo-physical and photochemical understanding of component molecules can explain laser ablation dynamics. Nanosecond and femtosecond laser ablation is interpreted well in terms of photothermal heating and transient pressure effects, respectively. Consequently, as a possible mechanism we can exclude plasma state, where materials are ionized and many free electrons are produced, leading to complex dissociation processes

and giving small molecules, radical, and even atoms. We know in some cases how we can avoid chemical decomposition accompanying laser ablation, on which we have developed some new methodologies for organic matters. Laser ablation of organic materials should be a potential fabrication method to prepared nanometer-sized materials and structures, and here we summarize nanoparticle preparation as a typical example.

Most of laser ablation studies are conducted for surface and surface layer of materials in air and in vacuum, and resultant fabricated surfaces and prepared structures have not been studied. On the other hand, the fragmented and ejected materials were usually deemed to be dusts, and their morphology, structure, and property were not examined in detail. Actually it is not easy to collect small ejected fragments efficiently in air and vacuum. If we catch the ejected materials and characterize them, a new approach toward small nanomaterials formation is made possible. Along this idea we proposed solution laser ablation method to prepare organic nanoparticles in inert solution.<sup>59</sup> This method is based laser ablation of microcrystals in solvent. High intensity laser pulse irradiation induced fragmentation of the surface layers of the microcrystals and small ejected particles are dispersed in solvent, giving stable colloidal solution. Some results of quinacridone red dye in water are given in Figure 19, where color change upon ablation and the corresponding absorption spectral changes are presented. The particles are usually charged to some extent, so that they are dispersed stably without additives like detergent, polymer, and so on. This method is simple and easy as it does not need big facility and complex chemical processes. Furthermore the method is enabling us to control nanoparticle size, shape, crystal structure, and morphology by adjusting laser parameters and chemical conditions.<sup>60–74</sup>

**3.1 Nanoparticle Preparation of Dye Molecules.** Here, we describe our nanoparticles preparation of four dye compounds, whose chemical structure and abbreviated names are depicted in Figure 20, using nanosecond YAG laser as an excitation light source.<sup>73</sup> Their micrometer-sized crystalline powders were added into a poor solvent where no appreciable dissolution of those molecules was detected. Here the dye concentration was about  $5 \times 10^{-3}$  wt % by applying sonication, and the solvent composition was water/ethanol (7:1) for BY, water/ethanol (39:1) for BP and DR, and just distilled water for QA and AlPc. For all examined dye crystals, most of the initial microcrystalline powder sank down on the bottom of a cuvette before laser irradiation, and its supernatant was almost colorless. This means that dye molecules are hardly dissolved in the corresponding poor solvent, since all compounds have strong absorption in the visible wavelength region. The microcrystals were dispersed in poor solvents by stirring the mixture vigorously with a magnetic stirrer, and then exposed to the third harmonic of nanosecond YAG laser (355 nm, 7 ns, 10 Hz). The morphology of initial microcrystals and formed nanoparticles were examined with a scanning electron microscope (SEM), absorption spectra of the supernatants prior to irradiation and of the obtained colloidal solutions were measured with a spectrophotometer. The latter measurement due to color changes was even conducted from time to time during processing, which gives information of how nanoparticle preparation evolves. By irradiating the dispersed solution at the laser

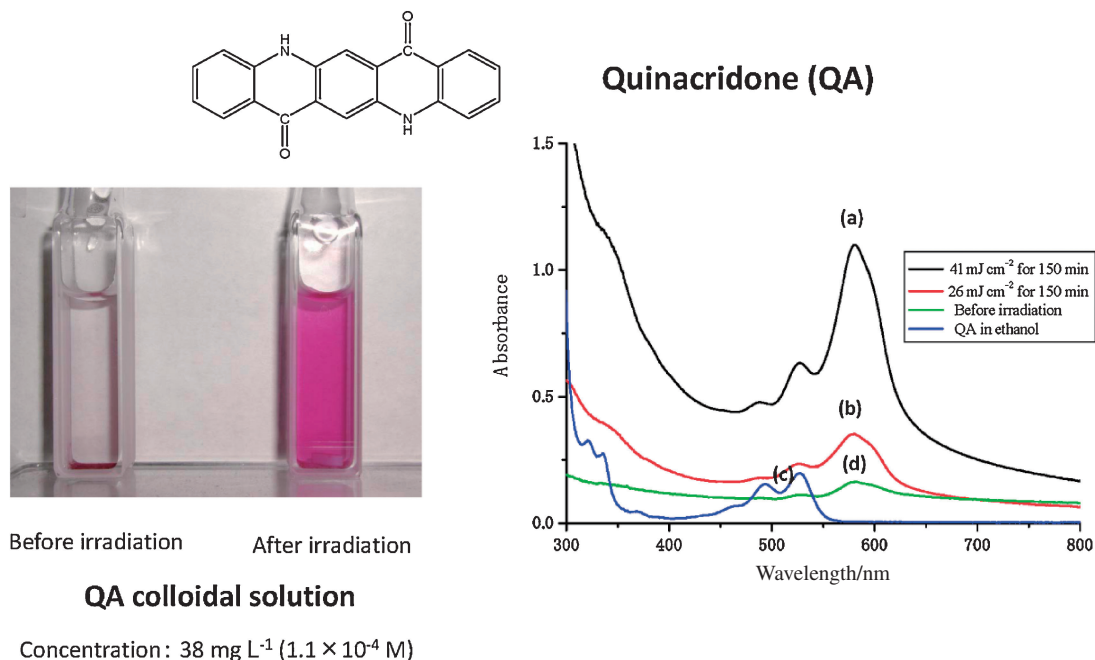


**Figure 19.** Chemical structure of quinacridone, and its solution color and absorption spectral changes upon solution ablation.

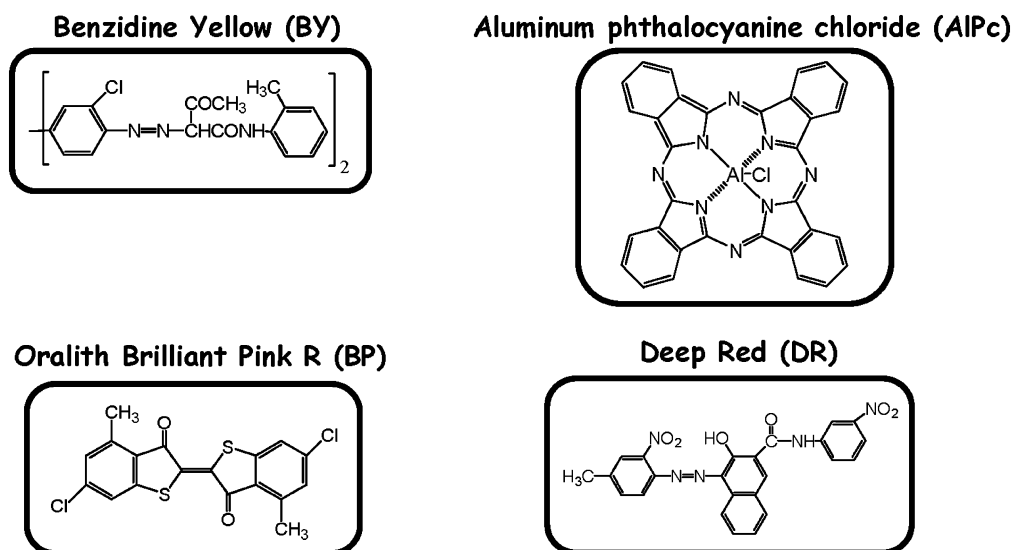


**Figure 20.** Chemical structures and abbreviation of dye compounds used for nanoparticle preparation.

fluence above the laser ablation threshold, the supernatant became colored and transparent by laser irradiation. Figure 21 shows the absorption spectra before and at 1 h after 5 min-laser excitation for QA, BY, AlPc, BP, and DR. The color solutions exhibited the characteristic absorption spectra of parent molecule, while they are more or less modified compared with the spectra of molecules fully dissolved in organic solvents. It is considered that dye molecules were dispersed in their poor solvents as their nanoparticles, because the solutions were colored and transparent with no tail in the visible wavelength region due to light scattering. The color of the colloidal solutions was observed for longer than a few weeks, although it gradually became pale due to their slow precipitation of nanoparticles.

To confirm nanoparticle formation more directly, SEM observation of the nanoparticles was performed, whose representative examples of AlPc, BP, and DR are given in Figure 22. It is interesting to see that small particles of the size of less than 100 nm are prepared from microcrystals just by laser pulse irradiation. In Table 1, the mean size and its distribution for each compound, and the thresholds of nanoparticle formation are listed. The mean size is ranged from 40 to 60 nm and independent of each dye, although their chemical structures and spectroscopic properties are quite different from each other. We also demonstrated similar solution ablation method by femtosecond laser and reported that femtosecond ablation gives smaller nanoparticle than nanosecond one. The size was 13 and 17 nm for QA and vanadyl phthalocyanine (VOPc), respec-

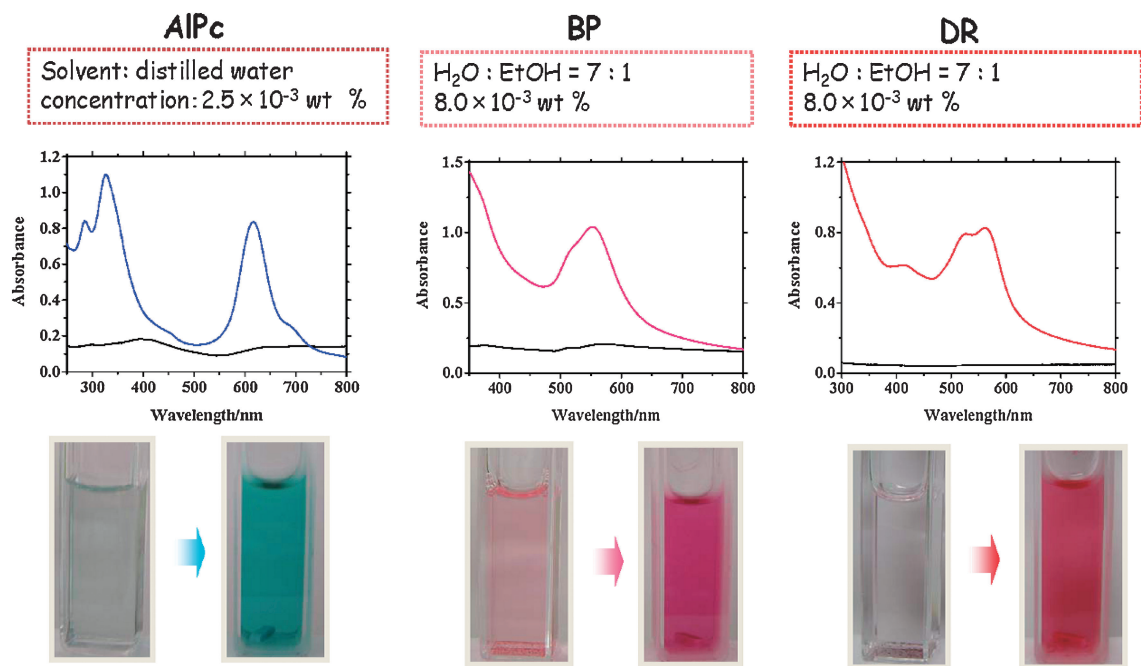


Figure 21. Solution color and absorption spectral changes of AlPc, BP, and DR.

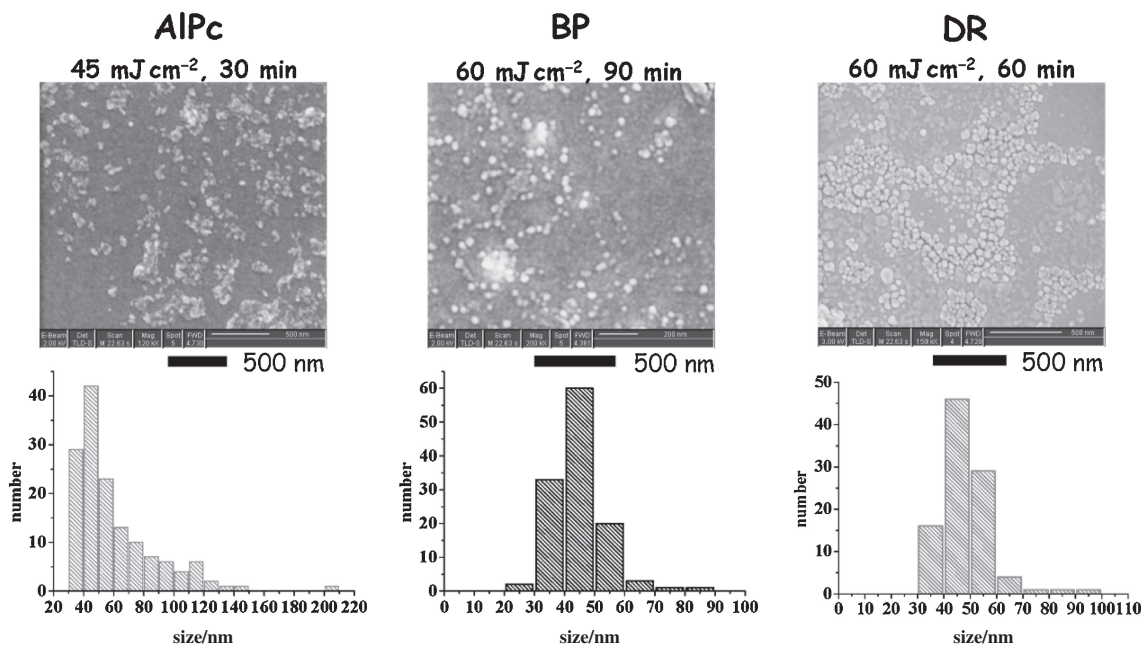


Figure 22. SEM observation of fabricated nanoparticles of AlPc, BP, and DR, and their size distribution.

tively, by using the femtosecond laser (780 nm, 200 fs FWHM) as an irradiation light source.<sup>62,72</sup> How nanoparticle size depends on laser pulse was confirmed for quinacridone in Figure 23. These experimental results indicate that the formed particle size is regulated by the pulse width of the excitation laser, which is applicable to various dye molecules.

We consider that nanoparticle formation mechanism is the same to ablation mechanism of polymer and dye films which we explained above. Laser-induced fragmentation of microcrystals should be due to photothermal laser ablation of organic solids in the case of nanosecond excitation. The excited states

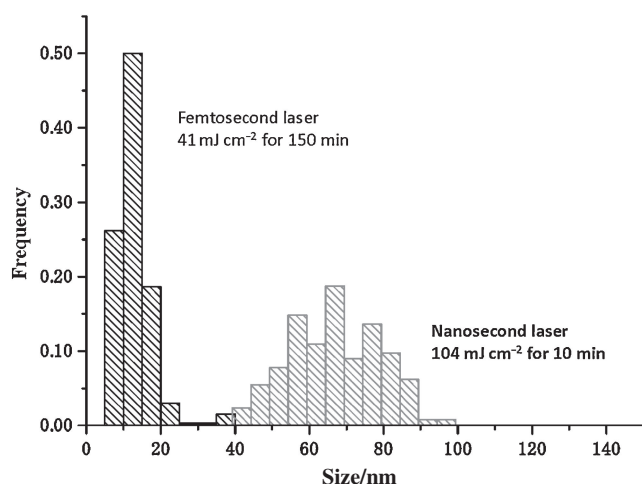
are densely formed in the irradiated area and undergo efficient mutual interactions leading to nonradiative relaxation. As this annihilation process is so rapid and much faster than original fluorescence decay process, the difference in nanoparticle lifetime between the dyes is not reflected in the nanoparticle size. Temperature jump at local irradiated area of crystals leads to fragmentation into small pieces, while temperature elevation of the area and ejected nanoparticles should be balanced by energy dissipation to solvent. We assumed that laser ablation is dependent on solvent cooling ability, which should be characteristic of solution laser ablation. Actually we confirmed

**Table 1.** Mean Size and Dispersibility of Dye Nanoparticles Fabricated by Solution Ablation with Its Ablation Threshold (See text)

	BY	AlPc	BP	DR	QA	VOPc
Mean size/nm (SD <sup>a</sup> )	59 (16)	56 (28)	40 (9)	43 (10)	50 (10)	49 (15)
Threshold/mJ cm <sup>-2</sup>	8	6	10	7	30	20
Dispersivity (Half-life of peak absorbance)	Longer than 13 days	Longer than 2 months	Longer than 6 days	Longer than 6 days	20 days	5 days

Light source: YAG laser (355 nm)      excimer laser (351 nm)

a) SD: standard deviation.

**Figure 23.** Size distribution of fabricated QA nanoparticles.

experimentally that the size of produced nanoparticle becomes smaller with the decrease in thermal conduction of the solvent.<sup>61</sup> Also the cooling rate for small particles should be faster than for large one because of their large surface-to-volume ratio. We consider that fragmentation proceeds until the temperature of the irradiated and fragmented materials is cooled down to the temperature at which thermal ablation does not occur anymore. The minimum particle size is thus determined by absorbed laser energy and dissipation to solvent. It is worth noting that femtosecond laser ablation in solution gives very small nanoparticles compared to the nanosecond excitation. This means that our method of laser ablation in solution enable us to form the smallest nanoparticles as a so-called bottom-up method.<sup>72</sup> It is reasonable to say that the femtosecond mechanism in solution is quite different from that of nanosecond ablation, so we consider that transient pressure mechanism is responsible to give the smallest organic nanoparticle of phthalocyanine dyes.

**3.2 Applications of Organic Nanoparticles Prepared by Laser Ablation in Solution.** Many applications are considered for those organic nanoparticles and here we describe some examples demonstrated in our laser laboratory. SEM pictures

of fullerene microcrystals and its nanoparticles prepared upon solution ablation are shown in Figure 24 with their size distribution. By changing irradiation condition of nanosecond laser, the concentration of the nanoparticle in solution can be controlled and the accompanying color change was clearly observed. The prepared solution is referred as a standard nanoparticle solution, as it is highly concentrated and very stable over for a few years without any additives.<sup>70</sup>

More direct and efficient application of the nanoparticles fabrication by solution ablation should be drug preparation. Usually the compounds designed and synthesized for medical use are complex and unstable, and sometimes they are not dissolved in aqueous solution. By adding detergents or by modifying chemical structures, the target compounds are dispersed under physiological aqueous conditions, but those results in some toxic effect and/or reduction in their original functionality. Our ablation method is just fit to such drug application, as we can disperse the target molecules as nanoparticles in water without any additives. Our preliminary trial was done for irinotecan hydrochloride for large intestine and lung cancers, drug for osteoarthritis,<sup>74</sup> myocardial infraction drug, and so on. The nanoparticles of these drugs are also stably dispersed in water, which is very useful for the next step biological examination for developing medicines.

The other application is to fabricate thin films from nanoparticles prepared by laser ablation. The fabricated nanoparticles can be regarded as an important building block to construct organic nanostructures for photonic and electronic devices.<sup>67</sup> Usually organic molecules and their self assembling structures, vacuum deposited thin films, and LB films were examined as building blocks. These are now quite conventional materials, but the prepared films are always suffering from the intrinsic defects, distribution of grain size, and so on. We prepared QA nanoparticles by the ablation method and then formed their films by utilizing electrophoretic method.<sup>66</sup> Fortunately QA nanoparticles are charged to be minus, which is the reason why the nanoparticles are dissolved in water without detergents, so they are attracted on to a plus-charged electrode giving flat film. These processes are schematically shown in Figure 25. It is interesting to see that size-, shape-, and phase-controlled nanoparticles prepared are used as a new building

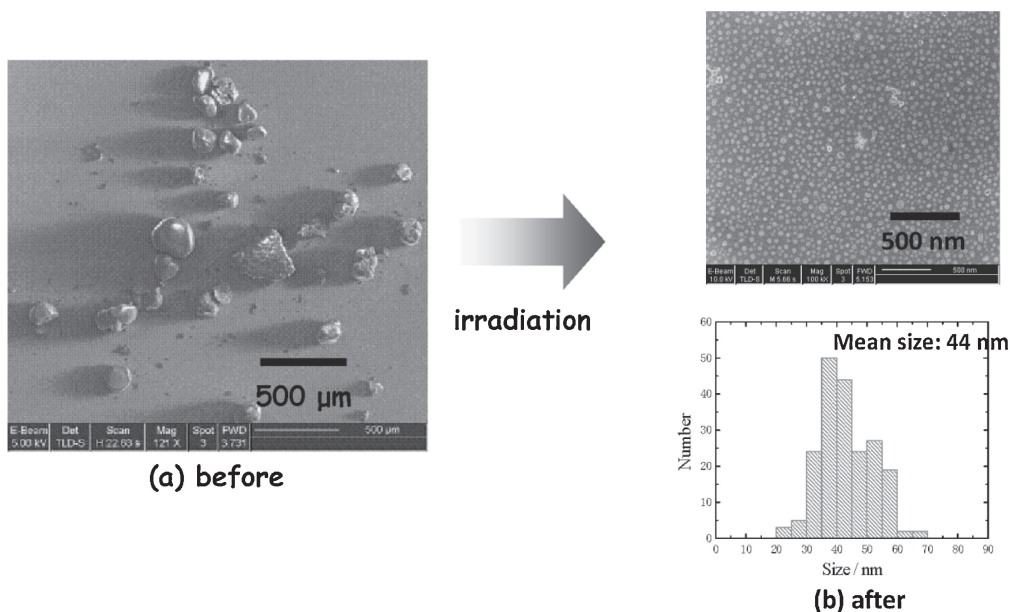


Figure 24. SEM observation of fullerene nanocrystals before and after the laser ablation, and their size distribution.

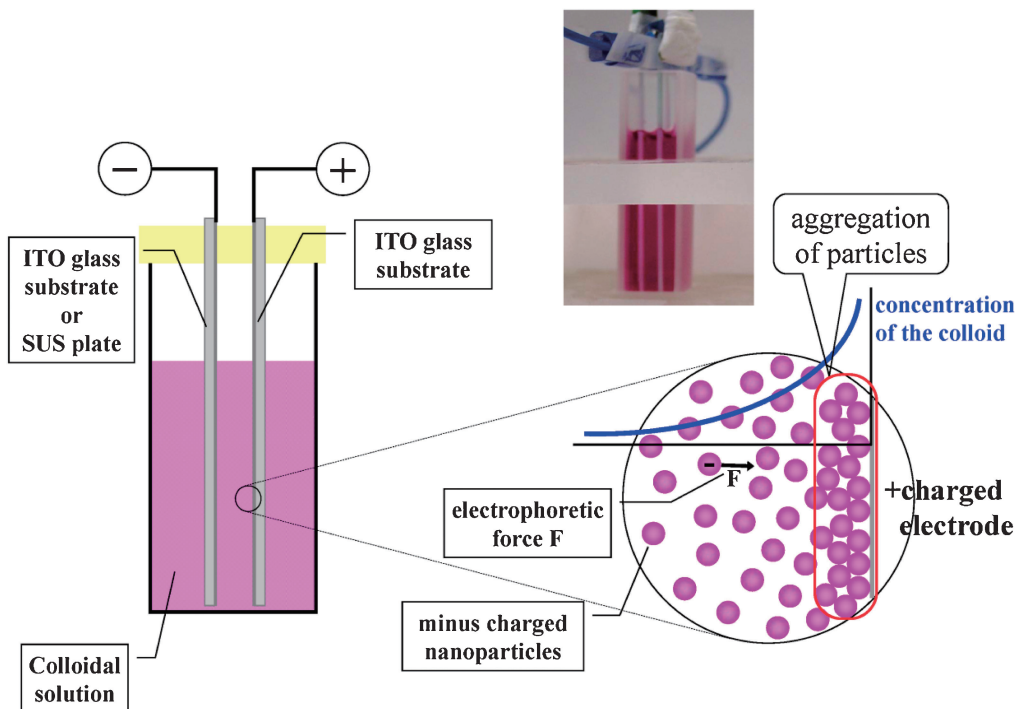


Figure 25. Experimental setup and illustration of electrophoretic deposition of QA nanoparticles.

block and transferred to very homogeneous films with new functionality.

#### 4. Crystal Growth in Solution by Femtosecond Laser Ablation

Laser ablation of molecular crystal in solution leaves its etched surface and gives nanoparticles, and both can be nuclei for crystallization if solution of the molecules is supersaturated. This possibility was demonstrated for the first time for aqueous solution of urea crystal.<sup>75</sup> When its single crystal prepared spontaneously by conventional way was irradiated by focusing

a single 800 nm femtosecond pulse, a quite novel phenomenon of crystal growth was observed. As shown in Figure 26, a needle-like crystal grew almost normally against to the mother crystal and its growth rate was estimated to be  $100 \mu\text{m s}^{-1}$ . Its needle shape is similar to that of the mother crystal which is characteristic of urea crystal. The subsequently prepared crystals tended to grow perpendicularly to the mother crystal, and the orientation of needle axis to the subsequent daughter crystal did not depend on polarization of the laser pulse. At the higher energy irradiation, several crystals grew near the irradiation area. The number of the daughters increased with

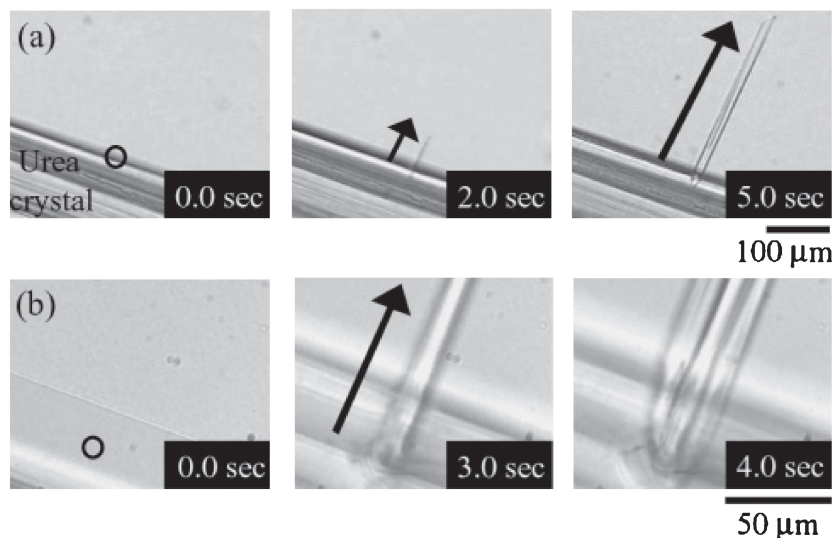


**Figure 26.** Subsequent crystal growth of urea from the irradiated area marked with an open circle by a single shot of (a) an 800 nm femtosecond laser pulse at  $0.12 \mu\text{J}/\text{pulse}$  through a  $10\times$  objective lens ( $\text{NA} = 0.4$ ), (b) an 800 nm pulse at  $0.030 \mu\text{J}/\text{pulse}$  through a  $20\times$  objective lens ( $\text{NA} = 0.46$ ). This figure is partly reproduced from Figure 1 of Ref. 75. Copyright 2013 American Chemical Society.

both the laser energy and the number of the pulse. These results are consistent with laser ablation behavior of molecular crystals. Upon every shot of laser pulse, ablation gives fragments and their number increases with laser fluence.

Etching and fragmentation of urea crystal are the origin of the crystal growth, which is strongly supported by AFM observation. The ablation of a urea crystal was carried out in air on the glass substrate and the obtained pictures are shown in Figure 27, where a hole etched in the crystal and fragments ejected on to the glass substrate are clearly identified. At higher laser fluence, many fragments with the size ranging from a few tens nm to a few  $\mu\text{m}$  were observed, and they spatially dispersed on the substrate. These fragmentations are considered to be caused by the transient pressure effect as explained in Sections 2 and 3, so that destructive thermal effect should be suppressed in this femtosecond ablation.

The present laser-induced crystal growth is unconventional and considered useful to form complex structures of crystals in supersaturated solution. The sequential irradiation gives something a set of blocks as shown in Figure 28. Another idea is to use this phenomenon to generate a new single crystal from multicrystalline or amorphous precipitates which are unfortunately formed. Sometimes proteins and newly synthesized compound are very expensive and/or difficult to get them again, so that repetitive trials to get single crystals should be very important, indeed, we succeeded in forming a new single crystal of lysozyme by ablation the mother crystal in saturated solution by a single shot femtosecond pulse.<sup>76</sup>

### 5. Multiphoton Laser Ablation of Solution Giving Local Impulsive Force

Multiphoton laser ablation is easily induced by focusing femtosecond laser pulse into water, leading to bubbling, which phenomenon should be started at the focal point, pushing the surrounding water toward its outside. This can cause local and transient pressure, which is similar to that in femtosecond

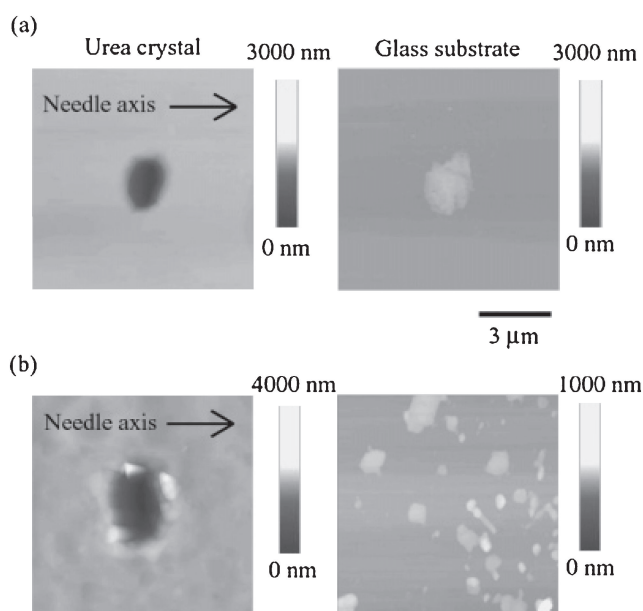


**Figure 27.** AFM images of the ablated fragments on a glass substrate (right) and the corresponding etched area of a urea single crystal (left) by single shot irradiation of an 800 nm laser pulse with (a)  $0.031$  and (b)  $0.056 \mu\text{J}/\text{pulse}$  through a  $20\times$  objective lens. Each image shows a  $10 \times 10 \mu\text{m}^2$  region. This figure is reproduced from Figure 4 of Ref. 75. Copyright 2013 American Chemical Society.

laser ablation mechanism as discussed. Consequently shock-wave is generated and propagates with high speed and local convection flow surrounding the focal point is induced. As a result mechanical force and water flow are loaded on small objects located surrounding the laser focus. This force is generated locally and temporarily in the three-dimensional space in solution, so that it is called local impulsive force. Then

the bubbles shrink, which is accompanied with local counter-convection flow. These multiphoton laser excitation behaviors are well known and have received much attention particularly for the biomedical subjects.<sup>13</sup> Most of the femtosecond laser applications, however, were carried out by focusing the femtosecond pulse to target materials, living cell, and so on.

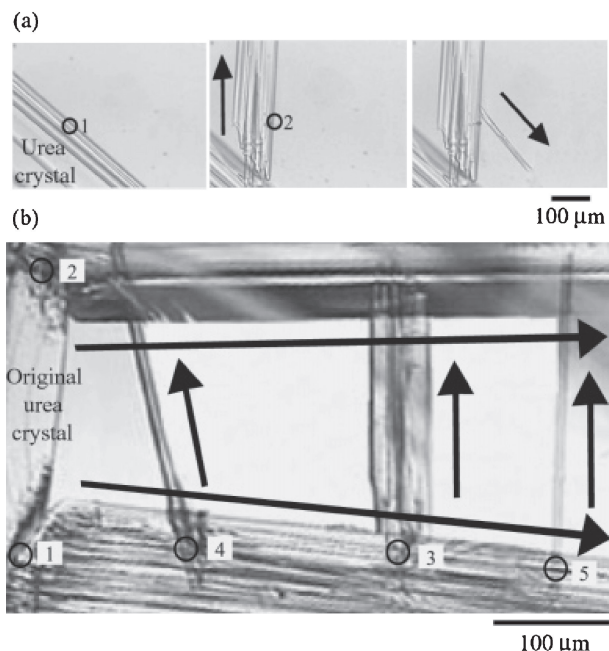


**Figure 28.** (a) Crystal patterning procedure for urea. The first pulse was irradiated to the open circle area numbered 1, the second pulse was to the circle 2, and so on. A single shot of the 800 nm femtosecond laser pulse with  $0.12 \mu\text{J}$ /pulse was irradiated through a  $10\times$  objective lens. (b) The ladder-like spatial pattern of urea crystals obtained by successive single shot laser irradiation of the five open circle areas each under the same irradiation conditions. This figure is reproduced from Figure 5 of Ref. 75. Copyright 2013 American Chemical Society.

In our case we do not irradiate the objects, but focus the pulse near the objects, and then the generated local impulsive force is used for their manipulation and processing.<sup>77</sup> This new method has an advantage that the target is not excited, no photophysical and no photochemical process is induced, and no damage is given. This has opened new ways in application of femtosecond laser ablation to manipulation and processing.

One application of the local impulsive force is to transfer a microparticle with the diameter of  $90 \mu\text{m}$  on a substrate in solution.<sup>78</sup> The femtosecond laser was scanned around the microparticle by using the scanning mirror to form a trapping circle, as shown in Figure 29. The trapping circle radius was set to  $150 \mu\text{m}$  and the scanning frequency was tuned to 10 cycles/s. The laser pulse energy was adjusted to  $5 \mu\text{J}$  and its repetition rate was set to 100 Hz, so that one cycle would consist of ten laser shots. A representative experimental result is shown in Figure 30, where we shifted the microscope stage. Small stains on a substrate moved clearly, but the target bead still remained in the center area of the trapping circle. Thus, it is obvious that the particle was trapped in the circle by the local impulsive forces from the surroundings. It is worth noting that a microparticle adhered to the substrate could be detached and moved easily. This method is applicable even to large microparticles which cannot be manipulated by conventional optical tweezers because of their limited trapping force.

We remember our former work on laser manipulation of  $\mu\text{m}$ -sized metal particles by a focused CW laser beam.<sup>79</sup> This beam exerts repulsive force upon optically reflective metal particles. As we are the first group to combine laser tweezers and beam scanning technique using Galvano mirror, we came to the proposal that a single metal particle should be surrounded by a circle locus formed by a scanning laser beam. As the force generates repulsive force, the metal particle was confined by the repulsive potential. This former idea is reproduced as a new manipulation method due to repulsive force, although its physical origin is different.

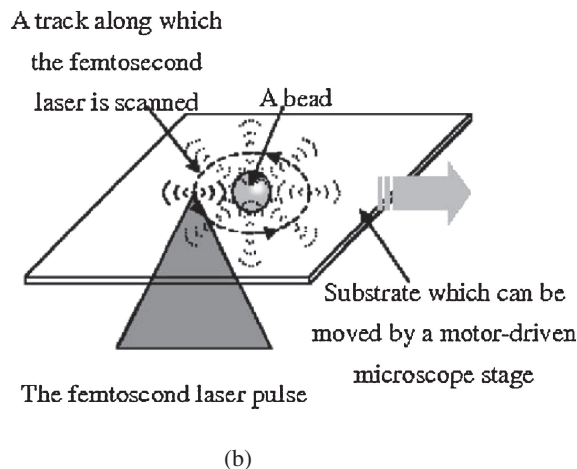
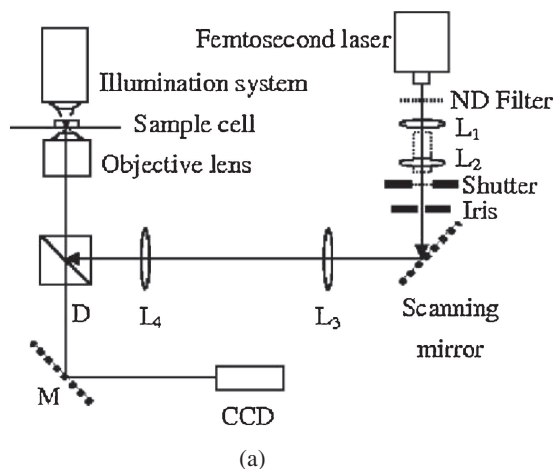


**Figure 29.** (a) Experimental setup for trapping and manipulation. The femtosecond laser beam was focused by a  $10\times$  objective. Laser focal point was controlled by scanning mirror and objective or L2 lens. (b) A trapping circle was formed by scanning the femtosecond laser beam around the target. Sample was moved by controlling the motor-driven stage. This figure is reproduced from Figure 1 of Ref. 78. Copyright 2013 American Institute of Physics.

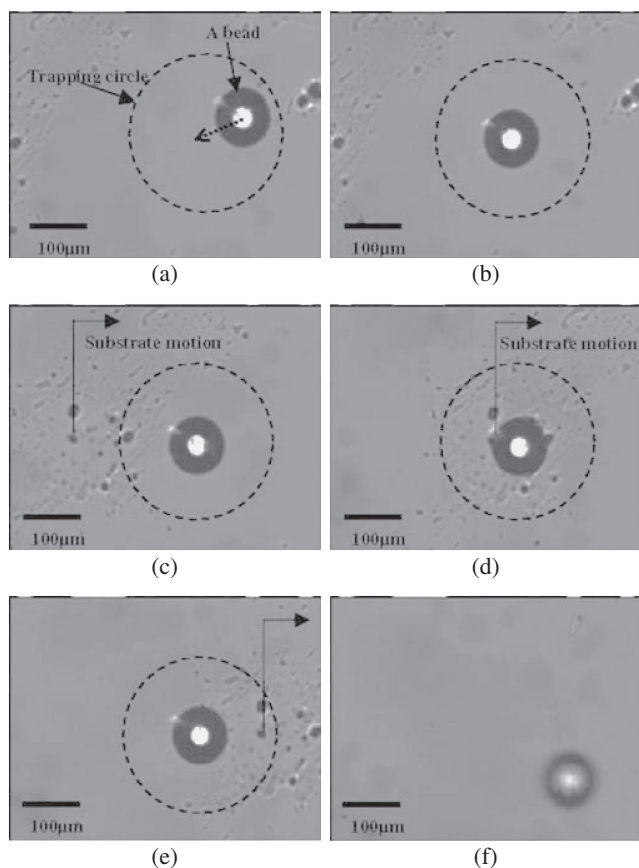


**Figure 30.** Trapping and manipulation of a single bead in water by the intense femtosecond laser irradiation. (a) Trapping is started by scanning the laser along the dotted circle; (b) the bead moves to the center of the trapping circle; (c)–(e) the bead is transferred laterally when the stage is driven, which is confirmed by the movement of the stains in the background; (f) the bead escapes from the trapping circle when the femtosecond laser irradiation is stopped. This figure is reproduced from Figure 2 of Ref. 78. Copyright 2013 American Institute of Physics.

The mechanical force induced by the impulsive force was estimated by analyzing the movement of the model bead, as shown in Figure 31. It is worth noting that the force exerted on the bead was estimated to be  $1 \mu\text{N}$  order and is extremely larger than that by the conventional laser trapping force (usually from pN to fN range). Quite recently Hosokawa et al. reports the precise determination of this mechanical force by utilizing AFM tip as a force sensor.<sup>80,81</sup> This femtosecond laser-induced force is transiently loaded and applicable only when the femtosecond laser was introduced, while the conventional laser trapping force by CW laser irradiation is constantly exerted. Another advantage of the laser-induced local impulsive force is that the target is not irradiated directly as mentioned above. The focal point is usually set to the position which is about  $10 \mu\text{m}$  far from the target. We can say that we have now two laser manipulation methods of conventional laser tweezers and the present manipulation by local impulsive force and can choose one of them or combine them depending upon a target and its condition.

## 6. Crystallization of Molecules and Proteins by Femtosecond Laser-Induced Local Impulsive Force

Laser-induced impulsive force is considered to be an effective stimulation to form nucleus in the supersaturated solutions of molecules and proteins. The propagating shockwave may increase local concentration temporarily and the local convection assists mass transfer giving higher local concentration. As a result, the system initially set in the meta-stable state may be shifted to crystallization area in the phase diagram (Figure 32) by the impulsive force and the convection. This idea explains the femtosecond laser-induced crystallization which we succeeded for the first time in 2002.<sup>82</sup> The molecule was lysozyme, a standard protein, and this femtosecond laser-induced crystallization is now extended to various kinds of molecules and proteins.<sup>83–90</sup> One typical example is on the 800 nm femtosecond laser irradiation of aqueous solution of egg-white lysozyme.<sup>83,84</sup> A similar experimental result was also reported by Watanabe et al.<sup>91</sup> Lysozyme crystallization is not difficult, but more efficient crystallization giving better quality compared to the conventional method was demonstrated. We considered that the bubbling induced by multiphoton laser ablation is responsible to lysozyme crystallization. In Figure 33, it is shown how crystallization proceeds on the bubble surface generated by the femtosecond laser irradiation.

Yoshikawa et al. examined effects of laser pulse energy and width, and reported that the threshold values of crystallization and the bubbling are similar to each other.<sup>92</sup> This indicates that the crystallization is started by the bubbling. As both laser bubbling accompanied with the impulsive force and crystallization are complex phenomena involving various processes, such an approach clarifying responsible parameters (in this case, the threshold) is very promising and is useful as the initial stage of research.

The questions we have received most frequently are on whether multiphoton excitation of the protein is involved or not. Namely photochemical reaction leading to less soluble species possibly triggers nucleation. Indeed Okutsu already reported interesting results, showing that photochemically formed tryptophan dimer is responsible to protein crystallization.<sup>93</sup> To make clear this issue we conducted an irradiation experiment shown in Figure 34. A single droplet of lysozyme aqueous solution was covered by paraffin oil and set on a microscope stage. The femtosecond laser pulse irradiated paraffin oil or aqueous solution with high intensity. In both cases bubble formation was observed and then some precipitants were identified. Namely laser-induced local impulsive force results in aggregation of proteins. In this experiment we set the condition to see visible  $\mu\text{m}$ -sized aggregates immediately after the irradiation, although crystals come at least after leaving the irradiated solution for a few hrs. Intense femtosecond laser pulse was introduced to the oil phase, while we confirmed formation of several bubbles not only in oil but also in protein solution. In several seconds the precipitant appeared in the aqueous solution. As the aqueous solution is not irradiated, this experiment clearly indicates that nondirect irradiation mechanism contributes to the crystallization. We consider that the shockwave propagates over the interface between both solutions in a droplet, forms bubbles, and triggers nucleation.

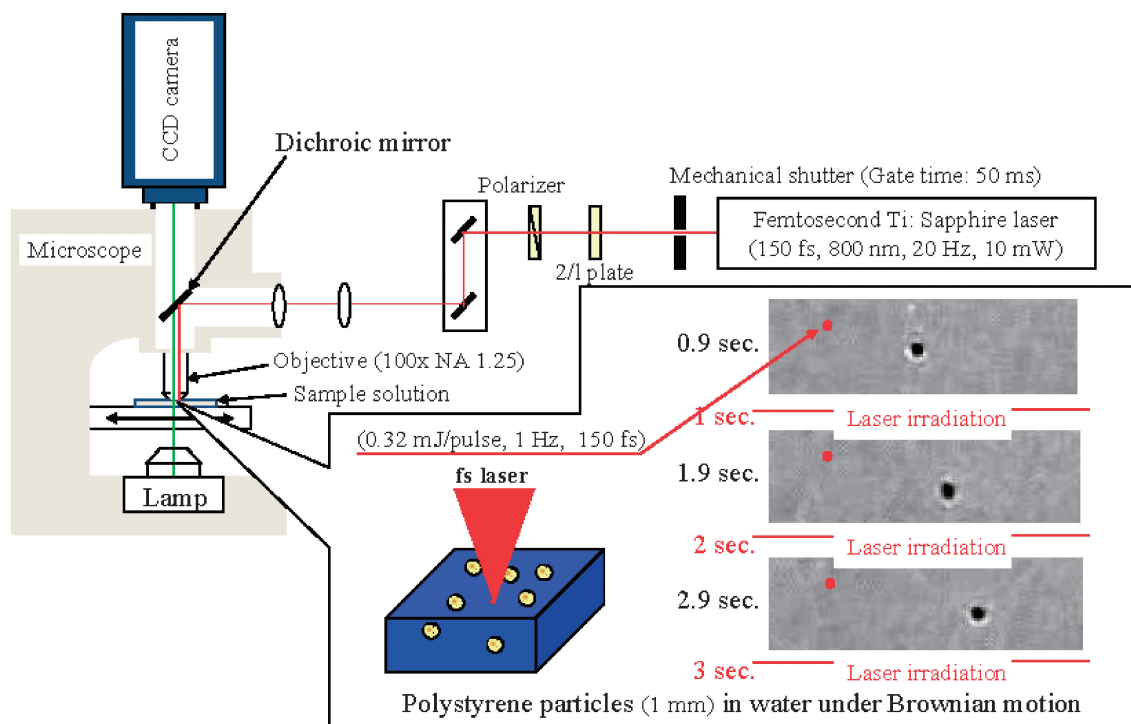


**Figure 31.** Optical setup, schematic illustration, and microphotographs of a single polystyrene nanosphere which was transferred by the local impulsive force.

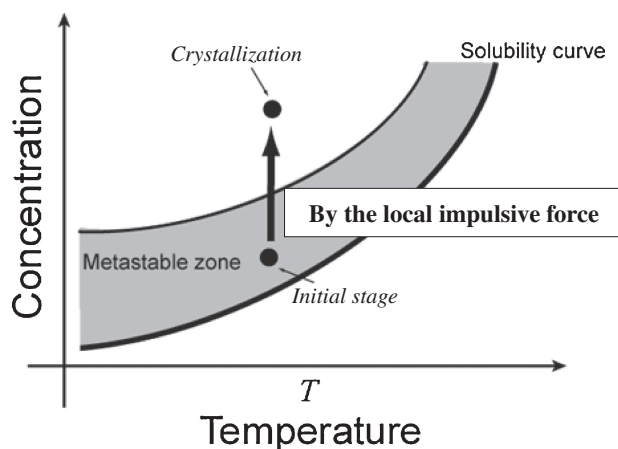


**Figure 32.** Schematic illustration of femtosecond laser-induced crystallization in phase diagram of crystallization.

A more direct confirmation of dynamics of this femtosecond laser-induced crystallization was demonstrated for simple solution system; anthracene in cyclohexane.<sup>89</sup> Its crystallization is very easy and crystal growth is fast, so that it is possible to monitor the growing within 1 s. A single shot femtosecond laser pulse with a pulse energy higher than above  $3.1 \mu\text{J}/\text{pulse}$  was irradiated into a sufficiently supersaturated solution, and then we found that anthracene crystallization was induced at the vicinity of the laser focal point immediately after the irradiation. The threshold of crystallization was in agreement with that of the laser-induced bubbling. The evolution of the crystal is pictured as in Figure 35, where a bending film-like crystal grew and changed to a normal shape. The bending form

strongly suggests that the nucleation and initial growth are started at the curved bubble surface, although the bubble disappeared already before 100 ms after the irradiation.

To confirm visually the role of bubbling in femtosecond laser crystallization, we show the spatial relation between bubbling and crystallization in viscous solution of hen egg-white lysozyme.<sup>90</sup> By adding poly(ethylene glycol) the viscosity is increased, so that we expect that the formed bubbles would not disappear soon and not diffuse out from the irradiated areas during the period necessary for crystal growth to visible size. Actually 1 day after the irradiation the lysozyme crystals were associated with bubbles and not so many crystals were found far from the bubbles. For an example, we could observe a long-lasting bubble with an initial diameter of  $120 \mu\text{m}$ . It shrunk to  $80 \mu\text{m}$  in 1 h and interestingly lysozyme crystals appeared at the surface of the bubble. This may also indicate that the surface is a preferential field for the crystallization. The long-lasting bubbles might be composed of gaseous molecules produced by photodissociation and photodegradation of solute and solvent due to multiphoton absorption at the focal point. In the present supersaturated solution, lysozyme and its clusters should be adsorbed at the surface and their ordering would evolve to nucleation, and furthermore the nuclei underwent to growth processes at the surface.

Similar approaches were adopted for clarifying crystallization processes of thaumatin protein. Yoshikawa et al. studied its femtosecond laser-induced crystallization by adding agarose gel. The gel enables us to monitor the crystal growth process from the focal point in the time range from  $\mu\text{s}$  to days. Crystals and bubbles were observed in the same area, which is ascribed to the suppressed diffusion of nuclei and bubbles. They also examined supersaturated lysozyme solution containing fluo-

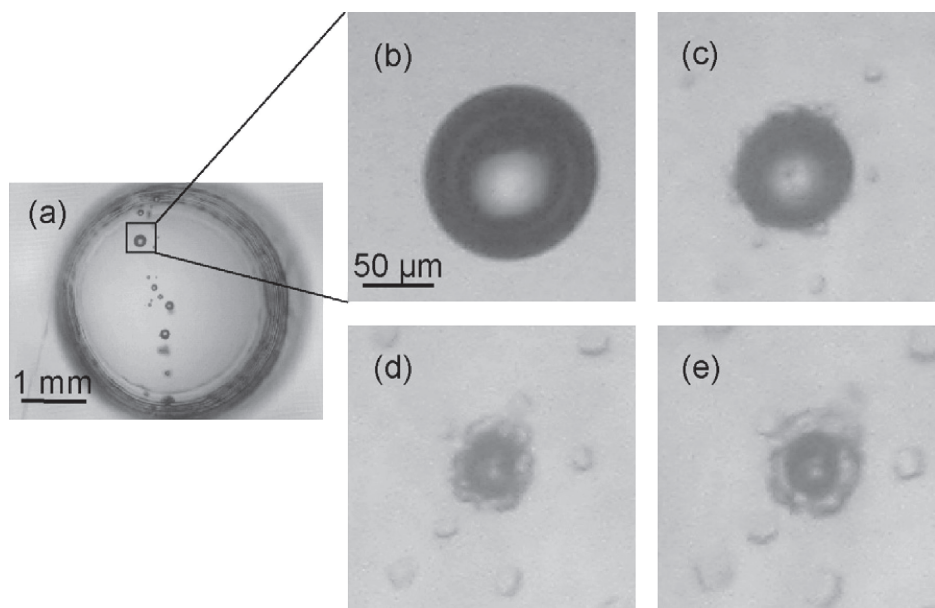


**Figure 33.** Time evolution of the HEWL crystallization at the surface of the long-lasting bubble created by a single scan irradiation with pulse energy of 30.0 mJ/pulse. These photographs were taken at (a) 0, (b) 1, (c) 3, and (d) 12 h, respectively. This figure is reproduced from Figure 3 of Ref. 90. Copyright 2013 Elsevier.

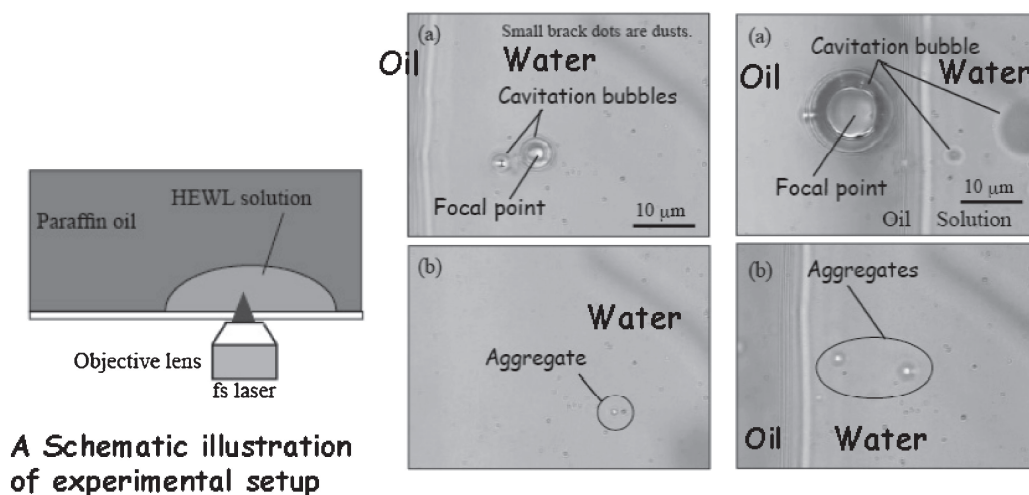


**Figure 34.** Lysozyme aggregation in water upon femtosecond laser-induced bubbling in paraffin oil.

rescent tetramethylrhodamine-5-isothiocyanate-labeled lysozyme by time-resolved fluorescence imaging. Initially a bright spot due to  $f_5$  laser-induced break-down was observed and the bubble underwent shrinking. Again a bright domain appeared around the focal point at 20  $\mu$ s after irradiation, which was interpreted as highly concentrated lysozyme. Namely, the shrinking of the bubble causes a local increase of the protein concentration, which is surely one possible reason of efficient nucleation.<sup>94</sup>

This femtosecond laser irradiation is useful to induce crystallization even under low saturation degree. Murai et al. demonstrated that the use of a gel solution with agarose-enhanced nucleation and produced egg white lysozyme crystals at 3 to 5 times lower saturation compared to the experiments without agarose and of spontaneous crystallization (without laser irradiation) with agarose.<sup>95</sup> Also their fluorescence imag-

ing of the labeled lysozyme revealed the cavitation bubbles formed the high concentration region at the focal point, which may trigger the nucleation similarly discussed above. The generated high concentration region remains longer in the agarose system, so the probability of nucleation should be increased. The present femtosecond laser crystallization method is improved by combining it with the solution-stirring technique,<sup>96</sup> and indeed this result has received much attention as a successful crystallization of membrane protein.<sup>97</sup>

### 7. Manipulation and Processing of Living Cells by Femtosecond Laser-Induced Local Impulsive Force

The femtosecond laser-induced impulsive force accompanying bubbling has high potential as a tool for managing single living cells in solution. We have devoted our efforts to explore new bubbling-induced behavior of living cells, on which we

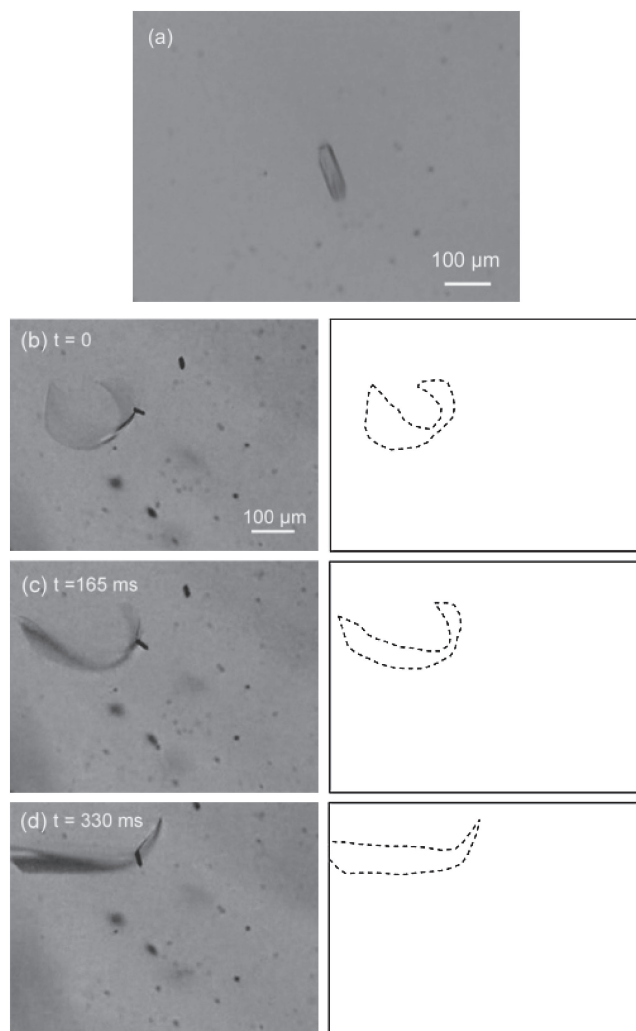


**Figure 35.** Microscopic images of generated anthracene crystals upon single shot femtosecond irradiation with energy of  $6.7\mu\text{J}/\text{pulse}$  (a) and its growth process of a bending film-like crystal generated at the surface of a large laser-induced bubble formed at a pulse energy of  $16.5\mu\text{J}/\text{pulse}$  (b–d). Right side illustrations represent generated crystals in left side photographs. This figure is reproduced from Figure 3 of Ref. 89. Copyright 2013 American Chemical Society.

have developed new manipulation methods.<sup>98–111</sup> As the laser is irradiated near the target, the living cells receive impulsive force but are not irradiated directly by the laser pulse. Also the intense force is loaded on the cells only transiently. These characteristics are complementary to laser tweezers where weak and constant force is exerted.

Here we start this text by introducing nondestructive isolation of single cultured animal cells.<sup>98</sup> Mouse NIH3T3 fibroblasts were cultured on a collagen matrix and its glass substrate with the matrix was placed upside down on an inverted microscope. Therefore a sample cell consists of the glass substrate with the matrix set upside down, solution, and a bottom glass substrate as illustrated in the right-upper illustration in Figure 36. The femtosecond laser was introduced through the bottom glass. Their filopodia were first cut by

convention femtosecond direct irradiation, namely by laser ablation, because cells are attached so strong that they cannot be removed by the impulsive force. Then the femtosecond laser was focused at a position about  $10\mu\text{m}$  from the matrix. The cells were detached individually from the matrix by the impulsive force and the laser bubbling. After that the cells fell down to the bottom through the solution and regenerated their filopodia on the bottom substrate, coming back to the original morphologies. It was estimated that the necessary force to realize this detachment was a few  $\text{N}\mu\text{m}^{-2}$ .

One important requirement for developing this femtosecond manipulation method as a general tool is to examine whether cell functions such as cell division, cell differentiation, cell death, and cell migration are damaged by the laser bubbling or not. The above detachment and regeneration is concerned with cell death, and actually we showed that, when NIH3T3 cells were detached from a collagen coated substrate, 80% of the cells adhered again on another substrate.<sup>99</sup> This percentage is comparable or higher than that of cells after reseeding by trypsin treatment. Another trial which we introduce here is to elucidate effects of the impulsive force on animal cell differentiation using PC12 cells derived from rat pheochromocytoma. A schematic illustration of our experimental procedure<sup>100</sup> is given in Figure 36. When nerve growth factor is interacted with PC12 cells, they are partially differentiated into neuron like-cells with neuritis. The differentiated and undifferentiated PC12 cells were selectively isolated by the bubbling and their morphological changes after falling onto the bottom substrate were compared. Upon isolation their neuritis were once contracted and some of them gradually regenerated day by day. When differentiated cells were isolated, the percentage of the differentiated cells with neurites at 6 h after isolation was about 3.3 times higher than that when undifferentiated ones were isolated. This result was comparable again with a control experiment where the isolation was carried out with trypsin treatment.

In view of cell division we studied dynamics of yeast fission cells and confirmed that the laser-induced local impulsive force does not damage their liability. Furthermore we applied this force to assist their fission. A similar enhancement of cell activity was demonstrated for cultured mammalian cells such as HeLa, PC12, P19CL6, and C2C12. They are stimulated by the impulsive force due to laser bubbling and their cell growth was examined. In comparison with the control condition, cell growth was enhanced for the cells of C2C12 and P19CL6, undergoing differentiation to myocytes. On the other hand a suppression effect was observed for the cell lines of PC12 and HeLa. These results suggest that cell growth is possibly enhanced for myogenic cells.<sup>101</sup>

Furthermore we have examined an effect of the impulsive force on cell migration, using melanocyte and keratinocyte in human skin tissue on a fabricated surface. The directional migration of melanocyte toward keratinocyte was directly observed, although the cells were arranged by the femtosecond impulsive force. This means that these cells were not negatively affected by loading the force.<sup>102</sup> Thus we consider that our laser manipulation method utilizing the local impulsive force is recognized to be useful not only from the viewpoint of laser fabrication but also as keeping cell functions during

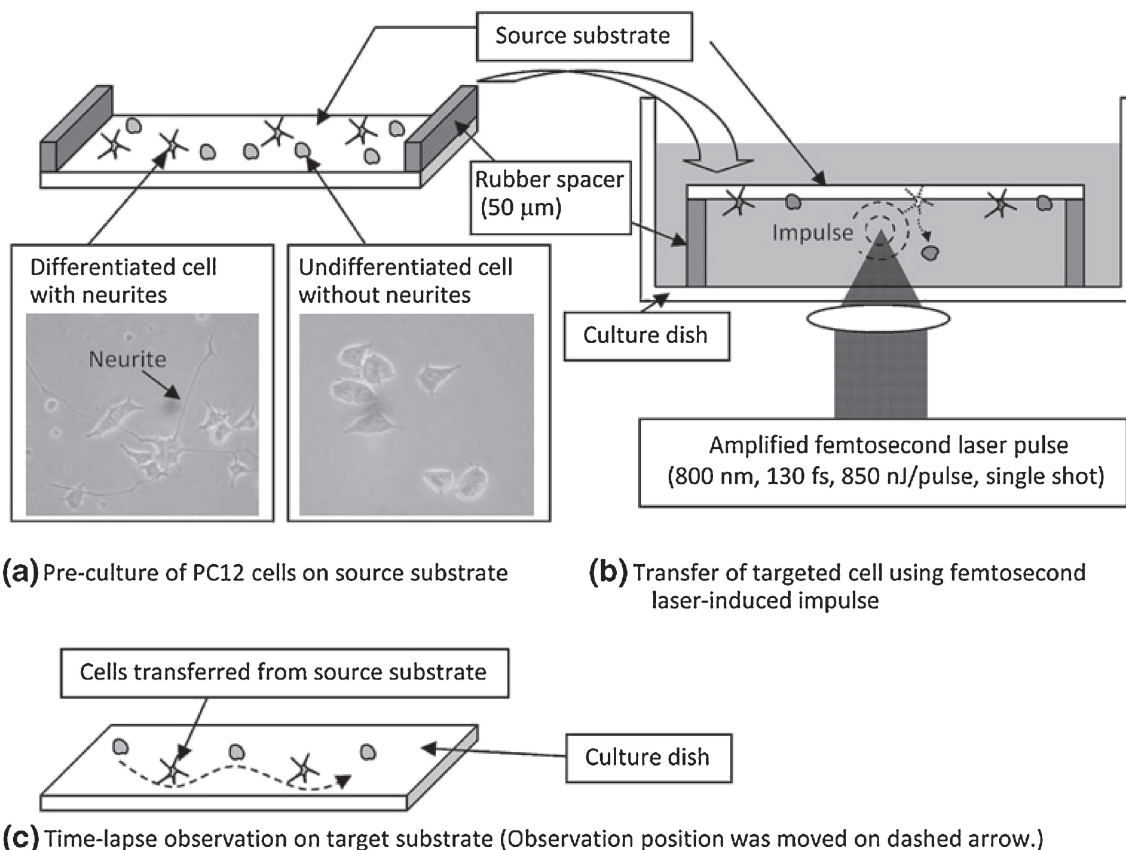


**Figure 36.** This figure is reproduced from Figure 1 of Ref. 100. Copyright 2013 Springer Publishing Co.

manipulation. To examine why the functions are well maintained during the removal, we cultured animal cells on a substrate which was coated a cell scaffold such as collagen. The cells were connected to the scaffold through cell adhesion molecules such as integrins and grown. As a conventional detaching method, trypsin was used and the detachment effect was compared with the result by the present femtosecond laser method. It is well known that the cell adhesion molecules are chemically digested where trypsin works as an enzyme. We studied both detachment methods in the single cell level by visualizing the scaffold with bright emission of quantum dots. When the cell was removed from the substrate by the laser bubbling, the emission simultaneously disappeared from the substrate. This means that the cell is detached together with the scaffold. On the other hand, only cells fell down and the scaffold showing the emission remained in the initial substrate upon the trypsin treatment. Thus we considered in the case of laser irradiation that the cell functions are well kept as they are surrounded by the scaffold.

The detachment technique was applied for various cells in different experiments. For example, the laser impulsive force was loaded to a substrate where PC12, HeLa, or normal human astrocyte (NHA) cells and the removed cells were translocated onto microfabricated cell-adhesive domains. The domains were prepared to be surrounded by cell-repellent surface, so that the patterning is well performed. By combining thus prepared cell patterns and additional femtosecond in situ fabrication, migration of HeLa or NHA cells along the fabricated channels was

examined. This approach will be useful not only to study the developing networks of neuronal, glial, and capillary cells, but also to the quantitative analysis of nerve function.<sup>103</sup>

The detachment by the impulsive force and accompanying bubbling was soon developed to a micropatterning method of living cells in solution. The mouse NIH3T3 fibroblast cells were detached from an upper substrate by the laser impulsive force and transferred to an underlying bottom substrate, which was fully conducted in water. By scanning the laser beam, consequently, shifting the bubbling, we can remove the cells along laser-scanned lines and curves, and transfer them to the target substrate, giving the similar lines and curves. The spatial resolution is not in the nanometer range, as laser-induced impulsive force is caused about 10 μm far from the cell and the diffusion from the source to target substrates are involved. The spatial resolution was estimated less than 80 μm in a full width at the half maximum. About 80% of the patterned cells were confirmed to be alive at 3 h after the process. It is considered that this technique is soft for biological materials as no exposure to the air is necessary. As a similar patterning method, inkjet printing, micro-contact printing, and laser-induced forward transfer in which a liquid droplet containing cells is ejected from a source substrate to target one by UV laser irradiation, are well known, but cells are more or less affected by air.<sup>99</sup> Our in situ patterning method is of course applied to other soft micrometer-sized materials in solution.<sup>104,105</sup>

The mechanical impulsive force is now applied to inject polystyrene nanoparticles in single living cells.<sup>106</sup> The nano-

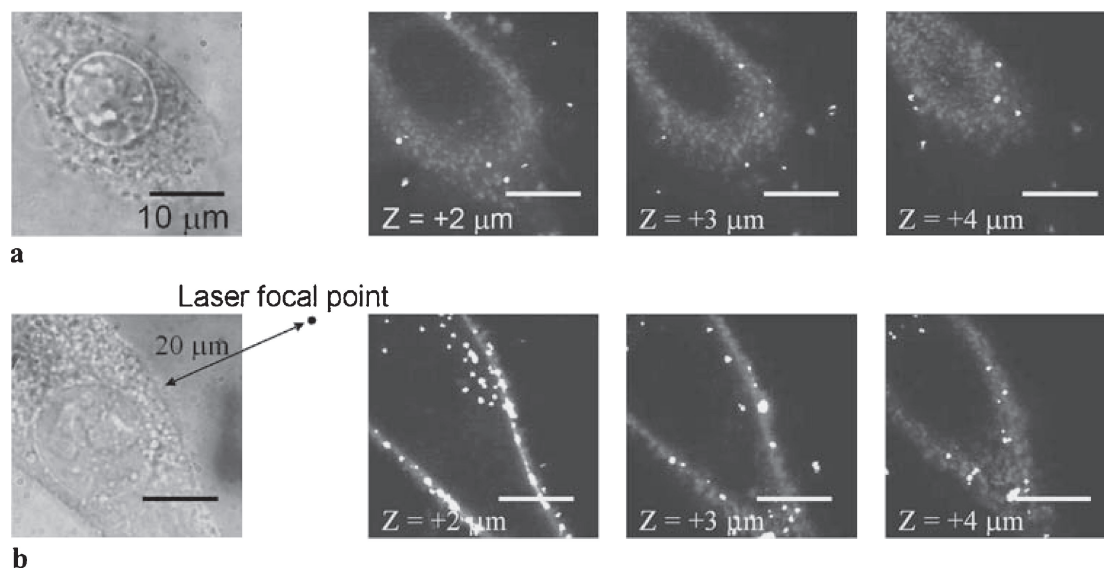


**Figure 37.** Transmission (left) and confocal fluorescence (right) images of a NIH3T3 cell at 10 min (a) before and (b) after adding polystyrene nanoparticles into the culture medium. The irradiation of 20 femtosecond laser pulses with focal spot size of 1  $\mu\text{m}$  were carried out at the laser focal point. Nanoparticles were absorbed on/in the cell membrane and their number increased with time, which may be due to electrostatic attraction between membrane (minus charge) and particles (plus charge). This figure is reproduced from Figure 3 of Ref. 106. Copyright 2013 Springer Publishing Co.

particles which are not soon absorbed are distributed on a living cell in solution and the femtosecond laser is focused near the cell, but not directly irradiated. A mouse fibroblast NIH3T3 cell was used, and the size of the focal point was 1  $\mu\text{m}$  and the distance between the focal point and the edge of the cell was 20  $\mu\text{m}$ . When the femtosecond laser was hit, the cell shrank a little, suggesting that its membrane structure should be changed at least transiently. The force exerted on the cell was estimated to be a few tens  $\text{fN}\mu\text{m}^{-2}$ , under which power the cell was not detached. The results are summarized in Figure 37.

The focal point was located in the top-right side of the cell. The bright spots observed at the right-upper and left-lower sides can be ascribed to the fluorescent polymer nanoparticles which we tried to introduce into a single cell. The confocal fluorescence image clearly shows, in addition to the particles on the stained membrane, that some particles are transferred into the inside of the cell and located close to the bottom but not on the bottom. Some bright spots look long shaped, suggesting the aggregation of the nanoparticles. The particle on the white lines (cursors) seems single, and its cross view along the  $z$ -axis is compared with those of the membrane stained with fluorescent dyes in Figure 37. Fluorescence intensity distribution of the stained dye has two peaks in the vertical profile, corresponding to the bottom and top surface membranes of the cell. On the other hand the fluorescence from the bead is located just between them, clearly indicating that the nanoparticles are injected into the cell.

## 8. Summary and Perspective

Initially laser ablation study of molecular systems was started from polymer films, as it received much attention as a key technology for future electronics. One of the mechanistic issues was concerned with plasma formation, as broad emission overlapped with sharp fluorescence peaks of diatomic radicals

and so on were usually observed. However, we considered that primary processes of laser ablation of molecular systems could be well explained in the framework of Jablonski diagram, developed various time-resolved imaging methods, and applied them together with time-resolved spectroscopy to polymer and dye films. It was proved that morphological changes evolving to fragmentation and ejection do not take place immediately after excitation and spectroscopic measurements of primary processes can be carried out as in conventional spectroscopy. Even under ablation condition we could identify excited singlet, triplet, and ionic states of chromophores which absorb excitation laser and confirmed that their dynamics are modified to large extent by high intensity excitation effects. Further plasma emission was demonstrated as the succeeding processes characteristic of laser fluence far higher than the ablation threshold.

Laser ablation is typical of molecular solids excited with high intensity laser pulse. Not only photophysical and photochemical dynamics but also the resultant morphological changes such as expansion and contraction, surface roughening, fragmentation to nanoparticles, and their ejection are sequentially induced, that is indeed solid-state photochemistry. Therefore our approaches integrating all the results obtained by time-resolved spectroscopic and imaging methods are very effective and we could clarify that photothermal, photochemical, or photomechanical dynamics is responsible to laser ablation depending on molecules and excitation conditions. Photothermal mechanism due to cyclic multiphotonic absorption for nanosecond laser ablation and transient pressure mechanism for femtosecond ablation was proposed and confirmed by us. Here we did not mention our systematic studies on laser ablation of neat liquid benzene and its derivatives, but it is worth noting that photophysical, photochemical, and photothermal processes induced by laser irradiation are directly correlated to morphological dynam-

ics.<sup>53,112–121</sup> The successful progresses in dynamics and mechanistic studies on laser ablation of molecular systems enabled us to develop unique methodologies which are seminal and applicable to material- and bio-sciences.

Molecular crystals in water are fragmented and ejected upon their laser ablation, and produced nanoparticles are dispersed well giving stable colloids. Their size usually ranges around a few tens nm, but it can be controlled by laser fluence, pulse width, repetition rate, wavelength, solvent, and temperature. The particle size of phthalocyanine dye fabricated by femtosecond laser ablation was 10 nm which is smallest as nanoparticles prepared by the top-down-method. The solution ablation method for nanoparticle preparation is contributing to emerging fields of nanoparticle science and technology,<sup>122</sup> as it is convenient in laboratory scale experiments.

When femtosecond multiphoton ablation of water, solution, and culture media for living cells is induced, impulsive force is generated due to bubble formation, shockwave propagation, and convection flow. The force is a very efficient perturbation for nucleation in supersaturated solution of molecules and proteins.<sup>123–125</sup> Our approach on femtosecond laser crystallization is now successfully developed and applied to more complex proteins.<sup>126–128</sup> The impulsive force can be loaded on individual cells by irradiating femtosecond laser at the position of about 10  $\mu\text{m}$  from the edge of cells. This means that the cells are not photoexcited and never photochemically damaged. Laser manipulation with the local impulsive force is very useful and applied to determine quantitatively cell–cell interaction force.<sup>81</sup> As a related method laser tweezers are well known, where the later trapping force is constantly loaded and its amplitude is in the fN–pN order. The impulsive force is transiently loaded and it reaches  $\mu\text{N}$ . Thus we consider that our manipulation due to femtosecond laser is complementary to the manipulation by laser trapping. In other words both manipulation methods are selectively utilized or integrated together to achieve complex manipulation depending on the biological targets.

In this Accounts we summarize our time-resolved spectroscopic and imaging studies of laser ablation, which convinces us that laser ablation is not a peculiar phenomenon but one of molecular photoprocesses under high intensity excitation. For further developments in the studies on laser ablation of molecules we plan to conduct the following subjects. 1) Simultaneous spectroscopic measurement and imaging to reveal how multiphoton excitation evolves to generate the local impulsive force. 2) Femtosecond electronic absorption spectroscopy of protein and amino acid solutions under femtosecond laser crystallization condition. 3) Separately we have been studying laser trapping crystallization by using CW laser,<sup>129</sup> where nucleation and the following crystal growth cannot be observed separately. By combining the present femtosecond crystallization with laser trapping crystallization, we will be able to control necessary concentration for nucleation and crystal growth and to adjust timing of nucleation independently. 4) The manipulation of living cells by the local impulsive force can be combined with laser ablation by direct irradiation, for example, protein patterning is achieved by the latter and the cells are transferred to the ablated area by the former. This approach in physiological aqueous solutions is believed promising for constructing future cell-based device. As conclusion molecular photophysical and

photochemical nature of laser ablation is being elucidated, which is a base for further developing new useful methodologies for material- and bio-sciences.

This study was partly supported by Japan Society for the Promotion of Science, Japan Science and Technology Agency, and Ministry of Education, Culture, Sports, Science and Technology Japan, and is now by MOE-ATU (Ministry of Education Taiwan - Aiming for Top University) Project of National Chiao Tung University, National Science Council Taiwan (No. NSC100-2113-M-009-001), and Foundation of the Achievement for Outstanding Scholarship Taiwan. The author thanks many colleagues and students whose names are included in the cited papers in the references, particularly to Prof. Hiroshi Fukumura (Tohoku University), Prof. Tsuyoshi Asahi (Ehime University), Prof. Yoichiroh Hosokawa (Nara Institute of Science and Technology), Dr. Teruki Sugiyama (Instrument Technology Research Center, Taiwan), and Dr. Kazunori Okano (National Chiao Tung University, Taiwan). Thanks are also due to Prof. Masahiro Irie (Rikkyo University) for his continued encouragement since 1969. The preparation of this manuscript is supported by Dr. Teruki Sugiyama.

## References

- # Dedicated to the late Prof. Noboru Mataga for his encouraging and stimulating the author by his research style.
- 1 R. Srinivasan, W. J. Leigh, *J. Am. Chem. Soc.* **1982**, *104*, 6784.
  - 2 D. Bäuerle, *Laser Processing and Chemistry*, Springer, Berlin, **2000**. doi:10.1007/978-3-642-17613-5.
  - 3 T. Lippert, J. T. Dickinson, *Chem. Rev.* **2003**, *103*, 453.
  - 4 T. Lippert, M. Hauer, C. R. Phipps, A. Wokaun, *Appl. Phys. A: Mater. Sci. Process.* **2003**, *77*, 259.
  - 5 R. Srinivasan, B. Braren, *Chem. Rev.* **1989**, *89*, 1303.
  - 6 G. Paltauf, P. E. Dyer, *Chem. Rev.* **2003**, *103*, 487.
  - 7 A. Vogel, V. Venugopalan, *Chem. Rev.* **2003**, *103*, 577.
  - 8 D. D. Dlott, S. Hambir, J. Franken, *J. Phys. Chem. B* **1998**, *102*, 2121.
  - 9 N. Bityurin, N. Arnold, B. Luk'yanchuk, D. Bäuerle, *Appl. Surf. Sci.* **1998**, *127–129*, 164.
  - 10 N. Arnold, N. Bityurin, *Appl. Phys. A: Mater. Sci. Process.* **1999**, *68*, 615.
  - 11 B. Luk'yanchuk, N. Bityurin, M. Himmelbauer, N. Arnold, *Nucl. Instrum. Methods Phys. Res., Sect. B* **1997**, *122*, 347.
  - 12 N. Arnold, B. Luk'yanchuk, N. Bityurin, *Appl. Surf. Sci.* **1998**, *127–129*, 184.
  - 13 N. Bityurin, A. Malyshev, *J. Appl. Phys.* **2002**, *92*, 605.
  - 14 S. Georgiou, A. Koubenakis, *Chem. Rev.* **2003**, *103*, 349.
  - 15 H. Masuhara, H. Hiraoka, E. E. Martinero, *Chem. Phys. Lett.* **1987**, *135*, 103.
  - 16 H. Masuhara, H. Hiraoka, K. Domen, *Macromolecules* **1987**, *20*, 450.
  - 17 H. Hiraoka, T. J. Chuang, H. Masuhara, *J. Vac. Sci. Technol., B* **1988**, *6*, 463.
  - 18 H. Fukumura, K. Hamano, H. Masuhara, *Chem. Lett.* **1993**, 245.
  - 19 H. Fukumura, K. Hamano, H. Masuhara, *J. Phys. Chem.* **1993**, *97*, 12110.
  - 20 H. Fukumura, N. Mibuka, S. Eura, H. Masuhara, N. Nishi, *J. Phys. Chem.* **1993**, *97*, 13761.

- 21 H. Masuhara, H. Hiraoka, K. Domen, *IBM Res. J.* **1986**, 5385, 55174\_1.
- 22 H. Fukumura, H. Masuhara, *Chem. Phys. Lett.* **1994**, 221, 373.
- 23 H. Fujiwara, T. Hayashi, H. Fukumura, H. Masuhara, *Appl. Phys. Lett.* **1994**, 64, 2451.
- 24 H. Furutani, H. Fukumura, H. Masuhara, *Appl. Phys. Lett.* **1994**, 65, 3413.
- 25 H. Fukumura, E.-i. Takahashi, H. Masuhara, *J. Phys. Chem.* **1995**, 99, 750.
- 26 H. Fujiwara, Y. Nakajima, H. Fukumura, H. Masuhara, *J. Phys. Chem.* **1995**, 99, 11481.
- 27 H. Fujiwara, H. Fukumura, H. Masuhara, *J. Phys. Chem.* **1995**, 99, 11844.
- 28 H. Furutani, H. Fukumura, H. Masuhara, *Rev. Laser Eng.* **1997**, 25, 288.
- 29 M. Hosoda, H. Furutani, H. Fukumura, H. Masuhara, M. Nishii, N. Ichinose, S. Kawanishi, *Rev. Laser Eng.* **1997**, 25, 306.
- 30 H. Masuhara, K. Sasaki, H. Fukumura, H. Furutani, *Analyst* **1998**, 123, 531.
- 31 H. Fujiwara, H. Fukumoto, H. Fukumura, H. Masuhara, *Res. Chem. Intermed.* **1998**, 24, 879.
- 32 T. Mito, T. Masubuchi, T. Tada, H. Fukumura, H. Masuhara, *J. Photosci.* **1999**, 6, 109.
- 33 T. Masubuchi, H. Furutani, H. Fukumura, H. Masuhara, *ChemPhysChem* **2000**, 1, 137.
- 34 T. Masubuchi, H. Furutani, H. Fukumura, H. Masuhara, *J. Phys. Chem. B* **2001**, 105, 2518.
- 35 T. Masubuchi, H. Fukumura, H. Masuhara, K. Suzuki, N. Hayashi, *J. Photochem. Photobiol., A* **2001**, 145, 215.
- 36 T. Mito, H. Masuhara, *Appl. Surf. Sci.* **2002**, 197–198, 796.
- 37 T. Tada, T. Asahi, H. Masuhara, M. Tsuchimori, O. Watanabe, *J. Photosci.* **2003**, 10, 97.
- 38 H. Fujiwara, H. Ishii, T. Ishiwata, T. Hayashi, H. Fukumura, H. Masuhara, *Bull. Chem. Soc. Jpn.* **2003**, 76, 1075.
- 39 T. Tada, T. Asahi, M. Tsuchimori, O. Watanabe, H. Masuhara, *Jpn. J. Appl. Phys.* **2004**, 43, 5337.
- 40 T. Tada, T. Asahi, M. Tsuchimori, O. Watanabe, H. Masuhara, *J. Nonlinear Opt. Phys. Mater.* **2004**, 13, 373.
- 41 H. Furutani, H. Fukumura, H. Masuhara, *J. Phys. Chem.* **1996**, 100, 6871.
- 42 L. Bennett, T. Lippert, H. Furutani, H. Fukumura, H. Masuhara, *Appl. Phys. A: Mater. Sci. Process.* **1996**, 63, 327.
- 43 T. K. Lippert, L. S. Bennett, T. Kunz, C. Hahn, A. J. Wokaun, H. Furutani, H. Fukumura, H. M. Masuhara, T. Nakamura, A. Yabe, *Proc. SPIE* **1997**, 2992, 135.
- 44 H. Furutani, H. Fukumura, H. Masuhara, T. Lippert, A. Yabe, *J. Phys. Chem. A* **1997**, 101, 5742.
- 45 T. Lippert, J. T. Dickinson, S. C. Langford, H. Furutani, H. Fukumura, H. Masuhara, T. Kunz, A. Wokaun, *Appl. Surf. Sci.* **1998**, 127–129, 117.
- 46 T. Mito, T. Tsujita, H. Masuhara, N. Hayashi, K. Suzuki, *Jpn. J. Appl. Phys.* **2001**, 40, L805.
- 47 T. Lippert, C. David, M. Hauer, T. Masubuchi, H. Masuhara, K. Nomura, O. Nuyken, C. Phipps, J. Robert, T. Tada, K. Tomita, A. Wokaun, *Appl. Surf. Sci.* **2002**, 186, 14.
- 48 T. Masubuchi, T. Tada, E. Nomura, K. Hatanaka, H. Fukumura, H. Masuhara, *J. Phys. Chem. A* **2002**, 106, 2180.
- 49 T. Lippert, J. T. Dickinson, M. Hauer, G. Kopitkovas, S. C. Langford, H. Masuhara, O. Nuyken, J. Robert, H. Salmio, T. Tada, K. Tomita, A. Wokaun, *Appl. Surf. Sci.* **2002**, 197–198, 746.
- 50 P. E. Dyer, J. Sidhu, *J. Appl. Phys.* **1988**, 64, 4657.
- 51 H. Furutani, H. Fukumura, H. Masuhara, S. Kambara, T. Kitaguchi, H. Tsukada, T. Ozawa, *J. Phys. Chem. B* **1998**, 102, 3395.
- 52 H. Van Mingroot, L. Viaene, M. Van der Auweraer, F. C. De Schryver, M. Ichikawa, H. Fukumura, H. Masuhara, *J. Phys. Chem.* **1995**, 99, 17174.
- 53 K. Hatanaka, T. Itoh, T. Asahi, N. Ichinose, S. Kawanishi, T. Sasuga, H. Fukumura, H. Masuhara, *Appl. Phys. Lett.* **1998**, 73, 3498.
- 54 Y. Hosokawa, T. Asahi, H. Masuhara, *Rev. Laser Eng.* **2001**, 29, 710.
- 55 Y. Hosokawa, M. Yashiro, T. Asahi, H. Fukumura, H. Masuhara, *Appl. Surf. Sci.* **2000**, 154–155, 192.
- 56 Y. Hosokawa, M. Yashiro, T. Asahi, H. M. Masuhara, *Proc. SPIE* **2001**, 4274, 78.
- 57 Y. Hosokawa, M. Yashiro, T. Asahi, H. Masuhara, *J. Photochem. Photobiol., A* **2001**, 142, 197.
- 58 L. V. Zhigilei, B. J. Garrison, *Appl. Phys. A: Mater. Sci. Process.* **1999**, 69 (Suppl.), S75.
- 59 Y. Tamaki, T. Asahi, H. Masuhara, *Appl. Surf. Sci.* **2000**, 168, 85.
- 60 Y. Tamaki, T. Asahi, H. Masuhara, *J. Phys. Chem. A* **2002**, 106, 2135.
- 61 Y. Tamaki, T. Asahi, H. Masuhara, *Jpn. J. Appl. Phys.* **2003**, 42, 2725.
- 62 T. Sugiyama, T. Asahi, H. Masuhara, *Chem. Lett.* **2004**, 33, 724.
- 63 T. Asahi, K. Yuyama, T. Sugiyama, H. Masuhara, *Rev. Laser Eng.* **2005**, 33, 41.
- 64 T. Sugiyama, T. Asahi, H. Takeuchi, H. Masuhara, *Jpn. J. Appl. Phys.* **2006**, 45, 384.
- 65 H.-G. Jeon, T. Sugiyama, H. Masuhara, T. Asahi, *Jpn. J. Appl. Phys.* **2007**, 46, L733.
- 66 H.-G. Jeon, S.-i. Ryo, T. Sugiyama, I. Oh, H. Masuhara, T. Asahi, *Chem. Lett.* **2007**, 36, 1160.
- 67 H.-G. Jeon, T. Sugiyama, H. Masuhara, T. Asahi, *J. Phys. Chem. C* **2007**, 111, 14658.
- 68 R. Yasukuni, T. Asahi, T. Sugiyama, H. Masuhara, M. Sliwa, J. Hofkens, F. C. De Schryver, M. Van der Auweraer, A. Herrmann, K. Müllen, *Appl. Phys. A: Mater. Sci. Process.* **2008**, 93, 5.
- 69 T. Asahi, T. Sugiyama, H. Masuhara, *Acc. Chem. Res.* **2008**, 41, 1790.
- 70 T. Sugiyama, S.-i. Ryo, I. Oh, T. Asahi, H. Masuhara, *J. Photochem. Photobiol., A* **2009**, 207, 7.
- 71 K. Yuyama, T. Sugiyama, T. Asahi, S. Ryo, I. Oh, H. Masuhara, *Appl. Phys. A: Mater. Sci. Process.* **2010**, 101, 591.
- 72 T. Sugiyama, T. Asahi, *Chem. Rec.* **2011**, 11, 54.
- 73 T. Sugiyama, H. Takeuchi, T. Asahi, H. Y. Yoshikawa, Y. Hosokawa, H. Masuhara, Laser Fabrication of Nanoparticles and Crystals in Solution, Proc. PICALO (Pacific Int'l Conf. Appl. Laser & Optics), **2008**, pp. 807–812.
- 74 D. Ikegami, T. Iwai, S. Ryo, N. Gu, T. Sugiyama, I. Oh, H. Yoshikawa, N. Tsumaki, *Osteoarthritis Cartilage* **2011**, 19, 233.
- 75 H. Y. Yoshikawa, Y. Hosokawa, H. Masuhara, *Cryst. Growth Des.* **2006**, 6, 302.
- 76 H. Y. Yoshikawa, Y. Hosokawa, R. Murai, G. Sazaki, T. Kitatani, H. Adachi, T. Inoue, H. Matsumura, K. Takano, S. Murakami, S. Nakabayashi, Y. Mori, H. Masuhara, *Cryst. Growth Des.* **2012**, 12, 4334.

- 77 Y. Hosokawa, J.-i. Takabayashi, C. Shukunami, Y. Hiraki, H. Masuhara, *Rev. Laser Eng.* **2004**, *32*, 94.
- 78 Y. Jiang, Y. Matsumoto, Y. Hosokawa, H. Masuhara, I. Oh, *Appl. Phys. Lett.* **2007**, *90*, 061107.
- 79 K. Sasaki, M. Koshioka, H. Misawa, N. Kitamura, H. Masuhara, *Appl. Phys. Lett.* **1992**, *60*, 807.
- 80 T. Iino, Y. Hosokawa, *Appl. Phys. Express* **2010**, *3*, 107002.
- 81 Y. Hosokawa, M. Hagiya, T. Iino, Y. Murakami, A. Ito, *Proc. Natl. Acad. Sci. U.S.A.* **2011**, *108*, 1777.
- 82 H. Adachi, Y. Hosokawa, K. Takano, F. Tsunesada, H. Masuhara, M. Yoshimura, Y. Mori, T. Sasaki, *J. Jpn. Assoc. Cryst. Growth* **2002**, *29*, 445.
- 83 H. Adachi, K. Takano, Y. Hosokawa, T. Inoue, Y. Mori, H. Matsumura, M. Yoshimura, Y. Tsunaka, M. Morikawa, S. Kanaya, H. Masuhara, Y. Kai, T. Sasaki, *Jpn. J. Appl. Phys.* **2003**, *42*, L798.
- 84 H. Adachi, Y. Hosokawa, H. Masuhara, M. Yoshimura, Y. Mori, T. Sasaki, *Rev. Laser Eng.* **2004**, *32*, 84.
- 85 Y. Hosokawa, H. Adachi, M. Yoshimura, Y. Mori, T. Sasaki, H. Masuhara, *Cryst. Growth Des.* **2005**, *5*, 861.
- 86 M. Kashii, H. Kitano, Y. Hosokawa, H. Adachi, Y. Mori, T. Sasaki, H. Masuhara, K. Takano, H. Matsumura, T. Inoue, S. Murakami, K. Sugamoto, H. Yoshikawa, *Jpn. J. Appl. Phys.* **2005**, *44*, L873.
- 87 H. Y. Yoshikawa, Y. Hosokawa, H. Masuhara, *Jpn. J. Appl. Phys.* **2006**, *45*, L23.
- 88 Y. Takahashi, H. Adachi, T. Taniuchi, M. Takagi, Y. Hosokawa, S. Onzuka, S. Brahadeeswaran, M. Yoshimura, Y. Mori, H. Masuhara, T. Sasaki, H. Nakanishi, *J. Photochem. Photobiol., A* **2006**, *183*, 247.
- 89 K. Nakamura, Y. Hosokawa, H. Masuhara, *Cryst. Growth Des.* **2007**, *7*, 885.
- 90 K. Nakamura, Y. Sora, H. Y. Yoshikawa, Y. Hosokawa, R. Murai, H. Adachi, Y. Mori, T. Sasaki, H. Masuhara, *Appl. Surf. Sci.* **2007**, *253*, 6425.
- 91 S. Watanabe, S. Nagasaka, K. Noda, H. Tashiro, *Jpn. J. Appl. Phys.* **2004**, *43*, L941.
- 92 H. Y. Yoshikawa, R. Murai, S. Maki, T. Kitatani, S. Sugiyama, G. Sazaki, H. Adachi, T. Inoue, H. Matsumura, K. Takano, S. Murakami, T. Sasaki, Y. Mori, *Appl. Phys. A: Mater. Sci. Process.* **2008**, *93*, 911.
- 93 T. Okutsu, K. Furuta, M. Terao, H. Hiratsuka, A. Yamano, N. Ferté, S. Veessler, *Cryst. Growth Des.* **2005**, *5*, 1393.
- 94 H. Y. Yoshikawa, R. Murai, S. Sugiyama, G. Sazaki, T. Kitatani, Y. Takahashi, H. Adachi, H. Matsumura, S. Murakami, T. Inoue, K. Takano, Y. Mori, *J. Cryst. Growth* **2009**, *311*, 956.
- 95 R. Murai, H. Y. Yoshikawa, Y. Takahashi, M. Maruyama, S. Sugiyama, G. Sazaki, H. Adachi, K. Takano, H. Matsumura, S. Murakami, T. Inoue, Y. Mori, *Appl. Phys. Lett.* **2010**, *96*, 043702.
- 96 H. Adachi, A. Niino, S. Murakami, K. Takano, H. Matsumura, T. Kinoshita, M. Warizaya, T. Inoue, Y. Mori, T. Sasaki, *Jpn. J. Appl. Phys.* **2005**, *44*, 1365.
- 97 H. Adachi, S. Murakami, A. Niino, H. Matsumura, K. Takano, T. Inoue, Y. Mori, A. Yamaguchi, T. Sasaki, *Jpn. J. Appl. Phys.* **2004**, *43*, L1376.
- 98 Y. Hosokawa, H. Takabayashi, S. Miura, C. Shukunami, Y. Hiraki, H. Masuhara, *Appl. Phys. A: Mater. Sci. Process.* **2004**, *79*, 795.
- 99 T. Kaji, S. Ito, H. Miyasaka, Y. Hosokawa, H. Masuhara, C. Shukunami, Y. Hiraki, *Appl. Phys. Lett.* **2007**, *91*, 023904.
- 100 Y. Maezawa, K. Okano, M. Matsubara, H. Masuhara, Y. Hosokawa, *Biomed. Microdevices* **2011**, *13*, 117.
- 101 Y.-E. Kuo, C.-C. Wu, Y. Hosokawa, Y. Maezawa, K. Okano, H. Masuhara, F.-J. Kao, *Appl. Phys. A: Mater. Sci. Process.* **2010**, *101*, 597.
- 102 Y. Maezawa, Ph.D. Thesis, Nara Institute of Science and Technology, **2011**.
- 103 K. Okano, D. Yu, A. Matsui, Y. Maezawa, Y. Hosokawa, A. Kira, M. Matsubara, I. Liau, H. Tsubokawa, H. Masuhara, *ChemBioChem* **2011**, *12*, 795.
- 104 Y. Hosokawa, T. Kaji, Y. Hiraki, H. Mori, H. Masuhara, *Proc. SPIE* **2006**, *6108*, 610805.
- 105 Y. Hosokawa, T. Kaji, C. Shukunami, Y. Hiraki, E. Kotani, H. Mori, H. Masuhara, *Biomed. Microdevices* **2007**, *9*, 105.
- 106 A. Yamaguchi, Y. Hosokawa, G. Louit, T. Asahi, C. Shukunami, Y. Hiraki, H. Masuhara, *Appl. Phys. A: Mater. Sci. Process.* **2008**, *93*, 39.
- 107 Y. Hosokawa, R. Yasukuni, T. Kaji, A. Yamaguchi, S. Iguchi, T. Asahi, H. Masuhara, *Rev. Laser Eng.* **2007**, *35*, 430.
- 108 N. Takizawa, K. Okano, T. Uwada, Y. Hosokawa, H. Masuhara, *Proc. SPIE* **2008**, *6854*, 685411.
- 109 Y. Hosokawa, Y. Jiang, I. Oh, N. Takizawa, T. Uwada, K. Okano, H. Masuhara, *Proc. SPIE* **2008**, *6854*, 68541K.
- 110 K. Okano, N. Takizawa, T. Uwada, Y. Hosokawa, H. Masuhara, *Proc. SPIE* **2008**, *6854*, 685414.
- 111 Y. Maezawa, Y. Hosokawa, K. Okano, M. Matsubara, H. Masuhara, *Appl. Phys. A: Mater. Sci. Process.* **2010**, *101*, 127.
- 112 Y. Tsuboi, H. Fukumura, H. Masuhara, *Appl. Phys. Lett.* **1994**, *64*, 2745.
- 113 Y. Tsuboi, K. Hatanaka, H. Fukumura, H. Masuhara, *J. Phys. Chem.* **1994**, *98*, 11237.
- 114 Y. Tsuboi, H. Masuhara, *Rev. Laser Eng.* **1995**, *23*, 2.
- 115 Y. Tsuboi, H. Masuhara, *Rev. Laser Eng.* **1995**, *23*, 9.
- 116 Y. Tsuboi, H. Fukumura, H. Masuhara, *J. Phys. Chem.* **1995**, *99*, 10305.
- 117 K. Hatanaka, M. Kawao, Y. Tsuboi, H. Fukumura, H. Masuhara, *J. Appl. Phys.* **1997**, *82*, 5799.
- 118 Y. Tsuboi, K. Hatanaka, H. Fukumura, H. Masuhara, *J. Phys. Chem. A* **1998**, *102*, 1661.
- 119 K. Hatanaka, T. Itoh, T. Asahi, N. Ichinose, S. Kawanishi, T. Sasuga, H. Fukumura, H. Masuhara, *Chem. Phys. Lett.* **1999**, *300*, 727.
- 120 K. Hatanaka, T. Itoh, T. Asahi, N. Ichinose, S. Kawanishi, T. Sasuga, H. Fukumura, H. Masuhara, *J. Phys. Chem. A* **1999**, *103*, 11257.
- 121 K. Hatanaka, Y. Tsuboi, H. Fukumura, H. Masuhara, *J. Phys. Chem. B* **2002**, *106*, 3049.
- 122 *Single Organic Nanoparticles*, ed. by H. Masuhara, H. Nakanishi, K. Sasaki, Springer, Berlin, **2002**. doi:10.1007/978-3-642-55545-9.
- 123 *Nano Biophotonics, Science and Technology*, ed. by H. Masuhara, S. Kawata, F. Tokunaga, Elsevier, Amsterdam, **2007**.
- 124 *Nanophotonics: Integrating Photochemistry, Optics and Nano/Bio Materials Studies*, ed. by H. Masuhara, S. Kawata, Elsevier, Amsterdam, **2004**.
- 125 *Molecular Nano Dynamics*, ed. by H. Fukumura, M. Irie, Y. Iwasawa, H. Masuhara, K. Uosaki, Wiley-VCH Verlag GmbH & Co., Weinheim, **2009**, Vols. 1 and 2.
- 126 T. Tsukazaki, H. Mori, S. Fukai, T. Numata, A. Perederina, H. Adachi, H. Matsumura, K. Takano, S. Murakami, T. Inoue, Y. Mori, T. Sasaki, D. G. Vassilyev, O. Nureki, K. Ito, *Acta Crystallogr., Sect. F: Struct. Biol. Cryst. Commun.* **2006**, *62*, 376.
- 127 T. Kinoshita, I. Nakanishi, T. Terasaka, M. Kuno, N. Seki,

M. Warizaya, H. Matsumura, T. Inoue, K. Takano, H. Adachi, Y. Mori, T. Fujii, *Biochemistry* **2005**, *44*, 10562.  
128 T. Numata, Y. Ikeuchi, S. Fukai, H. Adachi, H. Matsumura, K. Takano, S. Murakami, T. Inoue, Y. Mori, T. Sasaki, T. Suzuki,

O. Nureki, *Acta Crystallogr., Sect. F: Struct. Biol. Cryst. Commun.* **2006**, *62*, 368.  
129 T. Sugiyama, K.-i. Yuyama, H. Masuhara, *Acc. Chem. Res.* **2012**, *45*, 1946.



Hiroshi Masuhara graduated from Tohoku University (1966) in Sendai and obtained Ph.D. degree from Osaka University (1971). He is a physical chemist working in multidisciplinary areas in departments of chemistry (Tohoku University), synthetic chemistry (Osaka University), polymer science and engineering (Kyoto Institute of Technology), applied physics (Osaka University), frontier bioscience (Osaka University), life science (Hamano Foundation), and materials science (Nara Institute of Science and Technology). In 2008 he joined Department of Applied Chemistry and Institute of Molecular Science of National Chiao Tung University in Taiwan as a Chair Professor. He was awarded Asian Photochemistry Association Award, Mukai Prize (2010), The Purple Ribbon Medal (2008), Porter Medal (2006), the Chemical Society of Japan Award (2005), Osaka Science Prize (1994), Chemical Society of Japan Award for Creative Work (1994), Moët-Hennessy-Louis-Vuitton International Prize “Science for Art” Da Vinci of Excellence (1993), and received Doctor Honoris Causa de Ecole Normale Supérieure de Cachan (2006). Now he is foreign fellows of Royal Flemish Academy of Belgium and the National Academy of Sciences India. He has published more than 500 papers and wrote/edited 19 books. In Taiwan he is extending seminal researches on (1) laser trapping crystallization of molecules and proteins and (2) molecular trapping phenomena by femtosecond laser pulses.